Numerical and Experimental Study on Pulse Propagation with Coupling Loss in Nonlinear Chiral Fiber Couplers

By

Dr. Demissie Jobir

A Final Research Report Submitted to Adama Science and Technology University

Adama, Ethiopia
May, 2024

Abstract

In this research, we present a more general theory to describe the propagation of beams through chiral nonlinear fiber couplers. Considering Post's constitutive relations and Maxwell's equations, we derive the generalized coupled chiral nonlinear Schrödinger equations (CCNLSEs). The CCNLSEs govern the evolution of left- and right-handed circularly polarized (LCP and RCP) components with joint action of chirality, dispersion, and nonlinearity. Using the Runge-Kutta method, the linear behavior for low-power continuous wave (CW) and the characteristics of nonlinear switching for high-power CW in the couplers are explored. The interesting role of chirality in regulating the behavior of the different components in the coupler is demonstrated in our simulation. We found that the chirality could provide an additional degree of freedom, which may find applications in design of such a kind of device used in optical communication and remote sensing. We have also studied the nonlinear switching characteristics directional fiber couplers experimentally.

Keywords: Fiber coupler, chirality, chiral nonlinear fiber couplers, coupled chiral nonlinear Schrodinger equations, power exchange

Acknowledgements

We would like to express my greatest appreciation to Applied Physics department, and School of Aplied Natural Science, Adama Science and Technology University, Adama, Ethiopia for giving opportunity and encouragement to propose the research proposal.

We would like to gratefully acknowledge Dr. Kero Jemal, Dean, SoANSc, ASTU, Adama, Ethiopia for his continuous encouragement throughout the research work. As well-wisher, his insight, observations and suggestions helped us to establish the overall direction of the research and contributed immensely to the success of the work.

We acknowledge Dr. Geleta Hundassa, Associate Dean for research and Technology Transfer, Adama Science and Technology University, Adama, Ethiopia for their support and suggestions during the process of the project.

We acknowledge the academic resource that we received from Adama Science and Technology University, Adama, Ethiopia giving us a comfortable and active environment for pursuing our research work.

Table of Contents

List of Figures

Lis of Acronyms

B	Magnetic flux density
D	Electric displacement
E	Electric field
H	Magnetic field
Z	Chiral parameter
Δ	Optical rotation
E	Dielectric constant
M	Permeability
OFC	Optical fiber communication
SCSM	Single-core single-mode
NLO	Nonlinear optics
ORD	Rotatory dispersion
CD	Kerr circular dichroism
NLSE	Nonlinear Schrödinger Equation
TDM	Time division multiplexing
WDM	Wavelength division multiplexing
SDM	Space division multiplexing
NLFC	Nonlinear fiber coupler
RCP	Right circularly polarized
LCP	Left circularly polarized
OA	Optical activity
CB	Circular birefringence
OR	Optical rotation
CD	Circular dichroism
CNLFC	Chiral nonlinear fiber coupler
CCNLSEs	Generalized coupled chiral nonlinear Schrödinger equations
RKM	Runge-Kutta method
SBF	Silica-based fiber
PMF	Polarization-maintaining fiber

NZDF	Non-zero dispersion fiber
DFF	Dispersion-flattened fiber
HNLF	Highly nonlinear fiber
REDF	Rare-earth-doped fiber
POF	Polymer optical fiber
MOF	Micro structured optical fiber
PCF	Photonic crystal fiber
MNF	Micro-nano fiber
DWDM	Dense wavelength division multiplexing
SNR	Signal-to-noise ratio
PBG	Photonic band gap
SPP	Surface Plasmon polariton
DNR	Double negative refraction
RH	Right-handed
LH	Left-handed
EM	Electromagnetic
SHG	Second harmonic generation
SFG	Sum frequency generation
DFG	Difference frequency generation
EO	Electro-optic effect
OR	Optical rectification
SPM	Self-phase modulation
XPM	Cross phase modulation
FDTD	Finite-difference time-domain method
ODEs	Ordinary differential equations

1. Introduction

1.1 Research Background

Optical fiber communication (OFC) is concerned with using light and optical fibers for the transmission of information over long distances at high bandwidths and with high quality [1]. Currently, long distances refer to thousand kilometers and high bandwidths designates to terabit per second (Tb/s) capacities [2,3]. In the information era, information exchange and transmission are the integral part of our daily life and learning. People are constantly using a variety of different communications exchanges such as voice, image and data communications. Considering the phenomenon of globalization allied with the constant growth of our species, more and better services of communications, i.e., higher data and larger bandwidth with lower cost over long distances arouses more attention [2,3] and so, light wave technology has been developed. In fact, most of fibers used in communication are the silica-based fiber. Actually, such a kind of fiber has many advantages over all the earlier developed transmission media like coaxial copper cable. The compactness in size, low loss, low cost, high transmission capacity with very high quality, and high immunity to electromagnetic interference from the environment are to mention a few merrily. Thus making optical fiber transmission system the backbone of the communication.

As a basic of the network, optical fiber communication technology has been made considerable development in the past decades. Approximately, all telephone conversation, internet packet, and cell phone call have to pass through the optical fiber from source to the receiver [3,4]. Nevertheless, still social progress requires information to improve the optical signal transmission capabilities in technology, thus requiring people to continue to study the optical devices with different performance, to develop technologies that are more effective.

Actually, the current capacity of a single-core single-mode (SCSM) silica-based fiber has reached a surprising degree like 100 Tb/s by using some techniques such as time division multiplexing (TDM) [3,4], wavelength division multiplexing (WDM) and space division multiplexing (SDM). In reality, it is not enough, to meet the increasing demand of people on information. We should develop new ways to enhance the communication capacity.

As one of the candidates of information distributors that of very vital in modern optical networks, the nonlinear fiber coupler (NLFC) controlled by light gradually become one of the basic components in all-optical fiber communication systems since proposed in the early 1980's by Jensen [1]. Intense light can change the portion of the distributed optical information among output ports by nonlinear effect, which is, in fact, forms a family of all-optical switches [2]. The nonlinear fiber couplers and its application have been presented systematically by Govind P. Agrawal [3, 4].

It should be pointed out that most of the fiber couplers, which are constructed by the ordinary symmetric materials, like silica-based fiber (SiO_2) [4] have been studied completely and become available commercially. However, there still exist some problems, such as the linear and nonlinear coupling in the chiral fiber couplers and the performance of corresponding devices. Therefore, it is very necessary to do research on nonlinear coupling characteristics in chiral fibers.

Over the past decades, the NLC arouse a considerable interest both at fundamental and applied level [2, 3]. The main concern of researchers focuses on the manipulation of light by light, such as all-optical switching and signal processing [2, 5]. The switching occurring in an NLC is a result of intensity portion change among the participating waveguides by the change in coupling environments [5].

In order to realize NLC based all-optical switches, we need high nonlinearity and low absorption materials. As a new candidate, the chiral material has better optical nonlinearity, high switching speed and less absorption loss [6]. The working principle NLC in such material depends on the molecular orientation of nonlinear mechanism. In this regard, chirality has many remarkable electromagnetic facts which linked with all phenomena accompanying the difference in the interaction of a chiral medium with left circularly polarized (LCP) and right circularly polarized (RCP) light [7]. Such materials may find applications in optic communication such as a waveguide, fiber [8] and derivative devices [8, 9], polarization mode converters and all-optical switches as couplers.

Chirality is a purely geometric concept which refers to the lack of symmetry of objects which cannot be superimposed on its mirror image either through translation or rotation [10, 11]. Such media are known for their optical activity (OA) including circular birefringence (CB)) linked with the optical rotation (OR) - an ability to rotate the plane of linearly polarized light,

and in absorption, which is related to a term of circular dichroism (CD) [12, 13]. These effects reflect the different responses of chiral media to LCP and/or RCP incident lights. OA and CD are different manifestations of the optical response of chiral media. OA relates to the rotation of the plane of polarization of a linearly polarized light beam, while CD denotes the difference in absorption of light with LCP or RCP .

In the chiral nonlinear fiber coupler (CNLFC), the polarization state of the light-sensitive chiral medium, showing the optical support LCP and RCP light. Therefore, CNLC or NLC based on chirality may possess different coupling properties comparing to the achiral fibers coupler one. The research shows that the light in fibers filled with chiral media will decompose LCP and/or RCP modes with different propagation coefficients [14]. For this reason, the chiral fibers possess many characteristics based on which a number of novel devices, including polarization switches, couplers and so forth can be developed. Nevertheless, it is very pity that a few of people have recognized the greater academic value of NLC using chiral fibers.

The motivation behind this research is to explore CNLFCs giving emphasis to chiral fibers in presence of linear and nonlinear effects. The fiber composed of such media should possess novel properties in linear and nonlinear aspects. We take the chiral fiber and its derivative devices as the research topic and hope it will be meaningful to explore the unique roles of chirality in tailoring the transmission characteristics of pulses.

It consists of two closely placed chiral optical fibers (see Figure 1.1) which result in overlapping modal fields using for all-optical switching and signal processing functions.

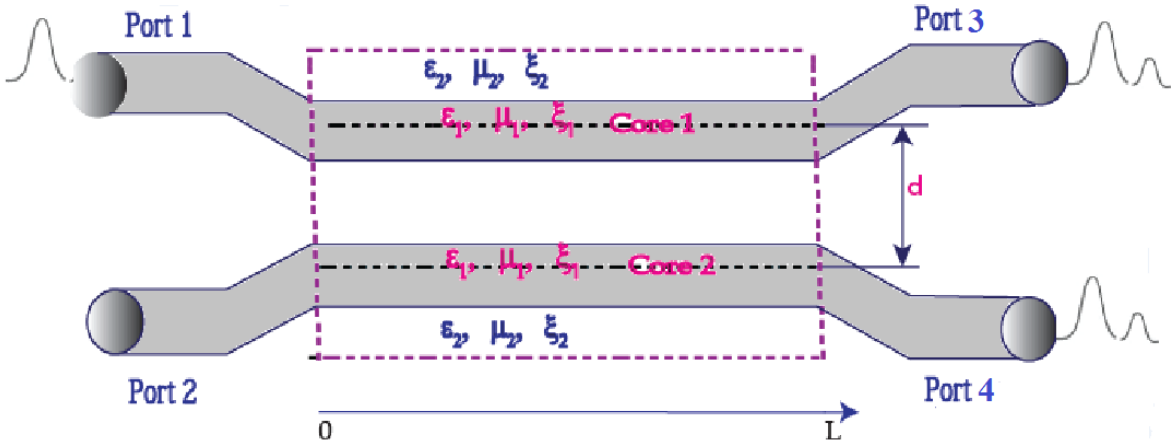

Figure 1.1 Schematic illustration of a nonlinear chiral fiber coupler

where $\mu_{1,2}$, $\varepsilon_{1,2}$ $\xi_{1,2}$ denote the permeability, permittivity, and chirality strength in the core and cladding, respectively with $\xi = 0$ meaning achiral medium.

1.2 Research Gaps

Principally, the current capacity for a single-core single-mode (SCSM) silica-based fiber by now reaches a surprising degree like 100 Tb/s by using some techniques such as time division multiplexing (TDM) [15], wavelength division multiplexing (WDM) and space division multiplexing (SDM). In fact, it is not enough in fact, to meet the increasing demand of people on information. We should develop new ways to enhance the communication capacity. As derivative fiber devices, chiral nonlinear coupler (CNLC) is the best candidate. The difference between the chiral fiber couplers and conventional counterparts lies in the different response to polarization. There are only two polarized modes in the traditional couplers but there are four polarized modes in the chiral fiber couplers.

In fact, the transmission characteristics of light pulse in traditional optical fiber have been studied and its applications and certain results have achieved, but for the CNLFC and other derivative fiber devices, it is just a beginning, there is a lot of work that need to be done. We believe that the following aspects of study are also very meaningful:

It is very important to demonstrate the behavior chirality in regulating the coupling and switching among the different components which may provide an additional degree of freedom to distribute the optical information that is very vital in optical communication and remote sensing by simulation.

It is worth to established generalized set of coupled chiral nonlinear Schrödinger equations (GCCNLSEs), which govern the evolution of LCP and RCP components in chiral fiber couplers for the treatment and numerical simulations.

To the best our knowledge, no previous investigations have reported how the presence of both dispersion and nonlinearities with the cooperation of chirality would affect the operation of CNLCs.

1.3 Objectives

1.3.1 General Objectives

The general objective of this research is to study chiral nonlinear fiber coupler (CNLFC) computationally and experimentally. We explore CNLFCs giving emphasis to chiral fibers in presence of linear and nonlinear effects.

1.3.2 Specific Objectives

In Order to accomplish the aforementioned general objective, we have the following specific objectives:

1) Develop a theoretical framework describing the transmission of optical pulses with two polarization components, LCP and RCP, simultaneously through chiral nonlinear fiber couplers (CNLFCs).
2) Establish the generalized coupled chiral nonlinear Schrödinger equations (CCNLSEs) based on which the evolution of LCP and RCP components can be discussed.
3) Simulate pulse propagation in chiral fiber coupling based on CCNLSEs using Runge-Kutta method.
4) Compute numerically and experimentally the power loss due to achiral fiber coupling.

1.4 Significance of this Research Project

Recent work on the fiber-capacity limit has indicated that the continued use of single-mode single-core silica-based fiber cannot afford the increase demand of information for modern communication systems. Although more single-mode fibers can be deployed as a short-term solution, it is important to develop new means of communication based on novel materials, novel structure and novel mechanism in order to meet the demand of high and quality information. Thus, we try to make our contribution in exploring new kinds of fibers and derivative devices based on some unique materials. Because of different response of chiral materials to opposite circularly polarized light, namely left- and right-handed circularly polarized (LCP and RCP) light, the fiber composed of such media should possess novel properties in linear and nonlinear aspects. In this research, the chiral fiber and its derivative devices are considered as the research topic and hope it will be meaningful to explore the unique roles of chirality in tailoring the transmission characteristics of pulses.

The significance of this research is concerned with the optical fiber based on the new material, the dielectric-chiral fiber. This is mainly due to:

1) In recent years, chiral fiber and derivative devices have attracted a great deal of researcher interest. The research shows that the light in fiber filled with chiral media will decompose LCP and RCP ones with different propagation coefficients. For this reason, the chiral fiber possesses a lot of characteristics which are different from that of the ordinary fiber, based

on which a number of novel devices, including polarization switches, polarization mode converter, sensors can be developed. 2) Nonlinear chiral fiber can find applications in optic communication such as a waveguide, fiber and derivative devices, all-optical switches, optical sensors and integrated optics devices. 3) Currently, because of the great applications as an optical signal processor, sampler, pulse compression, all optical switches, chiral nonlinear fiber couplers have attracted many of researchers' interests. We develop a more general theory to describe the propagation of beams through chiral nonlinear fiber couplers. We will show the role of chirality in the evolution of LCP and RCP components and its applications in all-optical switching. This is significant because it has applications in distributing optical information that is very vital in optical communication and remote sensing.

2. Literature Review

In the development, people have studied various kinds of optical fibers, such as silica-based fiber (SBF), polarization-maintaining fiber (PMF), non-zero dispersion fiber (NZDF), dispersion-flattened fiber (DFF), highly nonlinear fiber (HNLF), rare-earth-doped fiber (REDF), polymer optical fiber (POF). As the newly emerging fibers, micro structured optical fiber (MOF), photonic crystal fiber (PCF), micro-nano fiber (MNF), are intensively explored in a recent few decades, which are based on new transmission mechanism. From other aspect, the fibers based on the extraordinary materials including meta-material, negatively refractive material and chiral material also become the hot spots of research in academic community.

At the end of the 1980's people had proposed TDM [15]. Then around 1990's WDM gradually became the hot spot of research [16, 17] . After the coming of new century, the polarization division multiplexing (PDM) [18, 19] and SDM have received much attention in academic community with their power to increase the transmission capacity on the bases of currently existing optical communication frameworks. Moreover, the dense wavelength division multiplexing (DWDM) made more contribution to strengthen the spectral efficiency of the new window near 1.55 μm [20, 21] and to enhance the transmission capacity of the optical fiber.

As to the optical windows of fiber optic communication, they undergo three generations according to the attenuation of the silica-based fiber. For the first window the operating wavelength is about 850 nm. While the second window is located at 1310 nm. These windows were gradually replaced by the third window near 1550 nm because of relatively high transmission attenuation that is not suitable for long-haul optical communication and constructing backbone network. Besides, they don't have the corresponding online amplifying and dispersion compensating techniques [22]. The third window can provide a broader bandwidth with low absorption as well as it is suitable for DWDM and high gain rare-earth element doped fiber amplifier (REDFA) like erbium doped fiber amplifier (EDFA) [23].

However, the resources of third window gradually approach to the exhausted stage. According to the Shannon theorem [24], the improvement of signal-to-noise ratio (SNR) of optical signal transmission in optical fiber is not infinite and the space between the adjacent channels become extremely small. Moreover, the higher transmission power means the bigger nonlinear effects even fusing effect that can limit the capacity of single-mode single-core fiber.

This is the reason why we say that at the current level information transmission capability of the traditional single-mode single-core fiber has already reached its limit [24, 25]. We need new kind of fiber that can exceeds this limit to meet the increasing requirement for information capacity. Thus we should develop the fiber based on novel mechanism, novel materials and structures, which is just the current trends in fiber optic communication technology. We need even to reuse the first, second and third windows to completely enhance the optical communication capacity.

There are several mechanisms that can be used to construct new sort of fiber like photonic band gap (PBG) effect and surface plasmon polaritons (SPP) [26]. For some structure in which the micro-bodies (the solid rods, cylinders, even the holes) are arranged periodically in a fixed background. Because of periodicity of the structure, the Bragg scattering or diffraction may play the roles, which forms in fact a band gaps, i.e., frequency ranges over which electromagnetic wave propagation is prohibited for some directions and polarizations. The PBG materials possess an artificial hetero structures that enable controlling the generation of light and its direction. one can make use of PBG effect to confine the light and form new kind of waveguide.

The surface plasmon polariton is an electromagnetic mode formed by the interaction of free electrons and light fields near the interface of a dielectric and metal. The surface plasmonic field is the field tightly confined near the surface because of the evanescent property of the transverse field. The most of light may propagate only near the narrow range near the surface which is fact provide new wave guiding mechanism that can break through the diffraction limit and transmit light at a smaller spatial scale than the wavelength [27]. Due to the limitations of its transmission distance, micronano photonic waveguide mainly focus on the short-distance transmission and its derivative devices and their integration.

As new kinds of materials, the metamaterials [28, 29] and negatively refractive materials [15], which also includes chiral materials [15] have attracted the most attention in recent years. Metamaterials are materials that can be artificially designed and manufactured on the basis of nanotechnology. According to certain physical principles, they can be designed as novel and unique materials with some special properties that a natural material does not have. The structure of the monomer may decide the main properties of the material. With carefully designing the structure, the metamaterials may show the negative refraction and huge optical activity and perform some special functionality.

It should be pointed out that, there are mainly four ways to achieve the negative refraction.

Among the four ways, the double negative refraction (DNR), in which both the permittivity and permeability of the material should have negative values in some frequency ranges [30, 31] mainly performed by the metamaterials. In some special directions of the photonic crystal with special design even some crystals may also exhibit negative refraction [32, 33]. It is worth mentioning that for some materials when the chirality is strong enough that one of the components, namely the left or right circularly polarized (LCP or RCP) components experience a negative refraction in a certain frequency ranges [34].

Currently, the negative refraction is mainly realized by the metamaterials and even some materials with chiral structures. The negatively refractive material or medium has some interesting characteristics, such as reversed Cherenkov effect, reversed Doppler effect. This kind of material has a very attractive application prospects, such as superlens and invisible cloak [35], application in photonic crystal with complete band gap [36], total internal reflection type hollow [37], single interface waveguide [38], surface mode waveguide [39], non-mode waveguide [40] etc. It even be possible to get an optical fiber with negative refraction.

As a fiber with novel structures, photonic crystal fiber and structurally chiral fiber have received much attention.

Photonic crystal fibers consist of artificial periodic structures of dielectrics, which can be viewed as a sort of 2D photonic crystals with defect (as a future core of the fiber) or the fibers with transverse periodicity in which the light is confined to some range and has to propagate along the longitudinal but not the transverse direction. Due to the characteristics that photonic crystal fiber possess, which is not found in the traditional optical fiber, photonic crystal fiber has been paid great attention by the scientific community [15, 41].

Figure 2.1 shows a typical structure of photonic crystal fiber based on the triangular lattice of air holes, in which (a) and (b) correspond to the PCF with solid core and hollow core (also air hole), respectively. Photonic crystal fiber is different from the traditional fiber, it can be regarded as a class of periodic structure which is composed of two-dimensional photonic crystal with a specific defect, the defect part and other complete photonic crystal structure forms the core and cladding of the fiber, respectively.

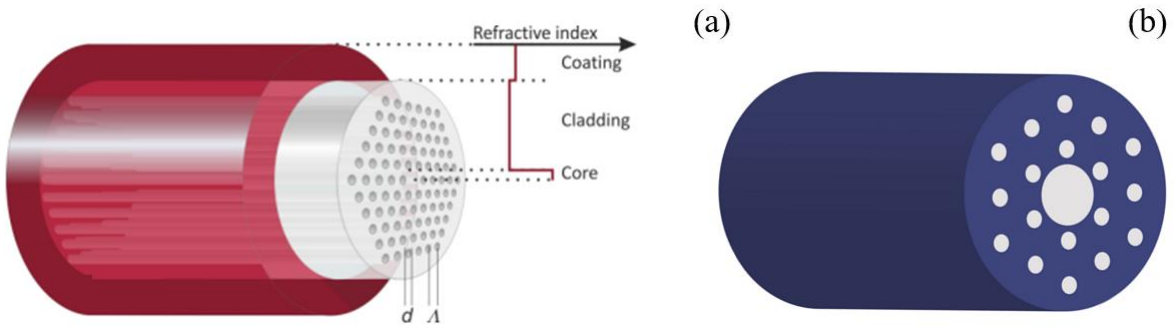

Figure 2.1 Schematic diagram of the PCF structures: (a) index guided type, (b) PBG type [42].

The structurally chiral fiber or the fiber with chirality (say a helical or twisted structure), which will be given a accurate definition in next section. Such a kind of fiber can be used to design circular-polarization-related components, such as the polarization-selective filter [43] and the generator of OAM [44] by twisting or with a spiral structure of the core or cladding [45, 46].

Figure 2.2 (a), (b), (c) and (d) give four examples of chiral structured fibers. In fact the first one is the twisted PCF, the second and the third ones are the fiber with helical surrounding attachment to the ordinary core and twisted ellipse core. While fourth one has Swiss roll like core. This kind of fiber with helix and twisted structure may provide a new degree of freedom to control the loss, dispersion and polarization state of light in optical fibers with noncircular guiding cores [47].

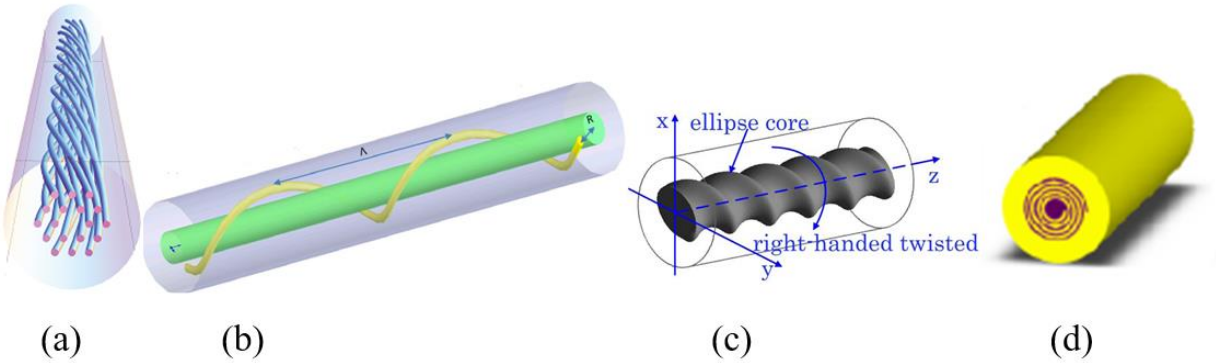

Figure 2.2 Schematic diagram of structurally chiral fibers [15].

2.1 Concepts of chirality and optical activity

Scientists have been fascinated by chirality, meaning right- or left-handedness, in the structure of matter ever since the concept first arose as a result of the discovery, in the early years of the nineteenth century, of natural optical activity in refracting media. The concept of chirality has inspired major advances in physics, chemistry and the life sciences [10, 48]. It is already

became a hot topic in nanoscience and is expected to stimulate further new and fruitful developments in technology.

A chiral medium is a macroscopically continuous medium composed of equivalent chiral objects that are uniformly distributed. A chiral object is a body that cannot superimposed on its mirror image with any real-space operation such as translation or rotation[10, 11]. The asymmetry of chiral bodies (say the chiral molecules) gives rise to optical rotation (OR), which is the ability to rotate the plane of linearly polarized (LP) light propagating through a chiral medium. This sort of medium with such objects has the property called as optical activity (OA). Chirality is equivalent with handedness, that means a chiral object must be either right-handed (RH) or left-handed (LH). An object that is not chiral is said to be achiral. Thus all objects are either chiral or achiral. The hands of a man is considered as the simple example of chiral objects. Actually, the word of chiral just comes from the Greek word "χειρ" (kheir) which means handed. Figure 2.3 shows a typical non-superposable chiral objects with their mirror images.

A chiral body can have two possible structures known as enantiomers, which are the mirror image of each others'. Such related objects are said to be enantiomorphism of each other. Simple example is the helix, which is one of the enantiomer with opposite handedness, i.e. LH or RH. By convention, the enantiomers are identified by their effect on linearly polarized light. When the observer faces the light source, the dextrorotary or (+) enantiomer rotates the plane of linearly polarized light clockwise, and the levorotary or (-) enantiomer rotates anticlockwise.

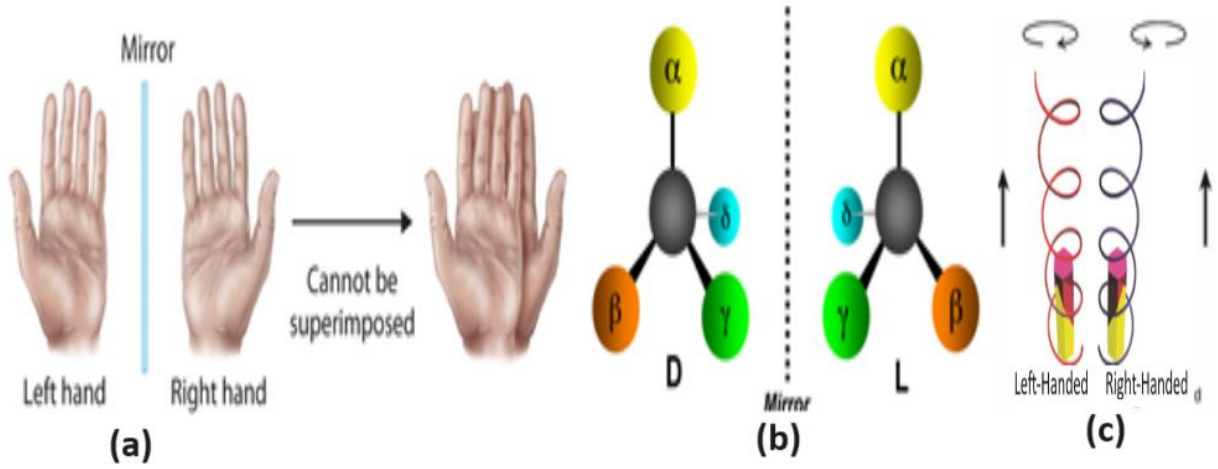

Figure 2.3 Classical definition of chirality as given by Lord Kelvin [49]: (a) Left and right hands and the left- and right handed molecules, (b) Alanine enantiomers and (c) spirals with left and right handedness.

The phenomenon of optical rotation is an example of circular birefringence (CB), with the material possessing a different refractive index for right-handed circularly polarized (RCP) and left-handed circularly polarized (LCP) light. Linearly polarized light entering the material is decomposed into RCP and LCP components, and its rotation is a result of these components traveling in the material at different phase velocities [15]. A sketch indicating circularly polarized light and their transmission states is shown in Figure 2.4. Fresnel had given the first successful explanation about the OA by using the decomposition of LP light into LCP and RCP light.

As mentioned above, the chiral material can perform differently [9, 50] for RCP and LCP components not only as a result of CB but also of circular dichroism (CD). CB and CD, in fact, are the two aspects of OA.

Circular birefringence (CB): From the obvious understanding, the word **CB** means having two refractions for opposite polarizations. CB is linked to OR - the ability to rotate the plane of polarization of electromagnetic waves. The CB reflects a behavior difference in refraction for RCP and LCP light. Usually the OR is one of the reciprocal process which does not depend on the polarization state of the incident wave and is the same for opposite directions of wave propagation, see Figure 2.5 (a). CB arises from different real parts of these refractive indices, which result in different phase delays for RCP and LCP components of an electromagnetic wave thus in polarization rotation.

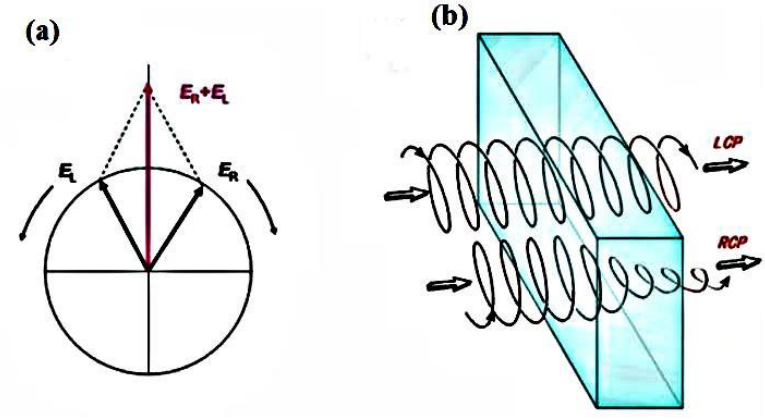

Figure 2.4 Circular birefringence and circular dichroism: (a) Illustration of the electric field rotation of LCP and RCP light and (b) Shows the image of LCP and RCP transmission [51].

Circular dichroism (CD): it corresponds to different transmission (or reflection) levels for RCP and LCP components. The behavior is identical for opposite directions of wave propagation, see Figure 2.5 (b). CD links to different imaginary parts of the refractive indices, which is related to the different absorption for circularly polarized light of opposite handedness.

(a) Circular birefringence (b) Circular dichroism

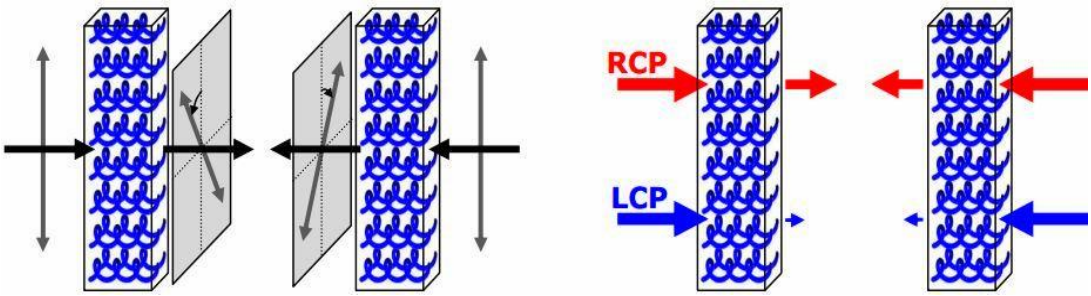

Figure 2.5 Polarization effects arising from 3D chirality: (a) Circular birefringence leads to rotating the plane of a linearly polarized electromagnetic wave and (b) Circular dichroism reflects the different transmission levels for LHCP and RHCP waves caused by different absorption [52].

According to Lord Kelvin's definition chirality can be classified into 3D and 2D, where the former describes the twisted nature of an object or structure like twisted structure say the helix, and some examples are shown in Figure 2.6 (a)-(c). It is widely accepted that materials with 3D-chiral symmetry shows the two important electromagnetic behavior, CB and CD. In contrast to 3D-chiral objects, 2D chiral (planar chiral) counterpart, which reflects the spiral nature of planar patterns like gammadion or S-elements, some examples are shown in Figure 2.6 (d)-(f). CB and CD due to extrinsic 3D chirality were recently observed in metamaterials by Plum E. et al group for the first time [53, 54].

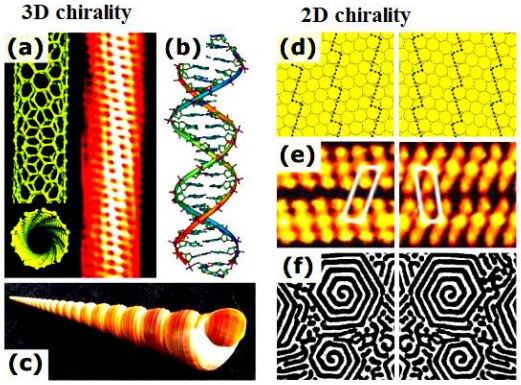

Figure 2.6 Examples of intrinsically chiral artiflcial and natural objects [52] 3D chirality: (a) single wall carbon nanotube (structure and tunneling electron microscope image), (b) DNA double helix and (c) seashell from the Turritellidae family. 2D chirality: (d) chiral surface of a gold monocrystal, (e) monolayer of (S, S)-tartaric acid (left) and (R, R)-tartaric acid (right) self-assembled on a copper surface and (f) surface of a metal-metal eutectic.

They were further investigated extrinsic chirality, provide the first experimental data on the optical manifestation of extrinsic 2D chirality and compare manifestations of 3D and 2D

extrinsic hilarities in a single series of parallel experiments. They also demonstrated optical activity in an intrinsically non-chiral anisotropic planar metamaterial. The phenomenon is due to extrinsic chirality resulting from the mutual orientation of the metamaterial structure and the incident electromagnetic wave.

2.2 Chiral material and structure with chirality

2.2.1 Dielectric chirality and structural chirality

According to the comparison between the size of the chiral structure and the size of the electromagnetic wavelength interested, the chirality can be categorized into the dielectric chirality and structural chirality. Correspondingly the materials may also be classified into two sorts, namely the dielectrically chiral ones and structurally chiral ones. When the size of the chiral object or structure is much smaller than the wavelength interested, the material composed of this sort of chiral things is called dielectrically chiral material, sometimes chiral medium, in which the chiral bodies are so tiny like as the chiral molecules as to the optical wavelength. On the other hand, if the size of the chiral object or structure becomes comparable with the wavelength of interest, the materials with chirality is called the structurally chiral ones. In general, only the dielectrically chiral medium can be described by a constitutive relation or matter equation which gives the response of the material to the external electromagnetic fields.

Figure 2.7 (a) and (b) show examples of chiral objects existing in nature, the first one indicates the chiral molecule and its enantiomer (the dissymmetric Centro-Carbon molecules) while the second one is the image for the left- and right-handed French snails, which, in fact, reflects the remains of microscopic chirality at macroscopic level. It should be pointed out that the chiral molecules can also be chemically synthesized. Figure 2.7 (c) and (d) demonstrate the artificially chiral bodies. The materials like polymers if doped with chiral molecules become chiral ones. Chiral materials with strong chirality strength are rare to find in nature. We often meet the chiral things in nature with relatively weak chirality. In fact, the chirality strength of material can be designed and modified even enhanced, which has become a hot spot in the material science and engineering.

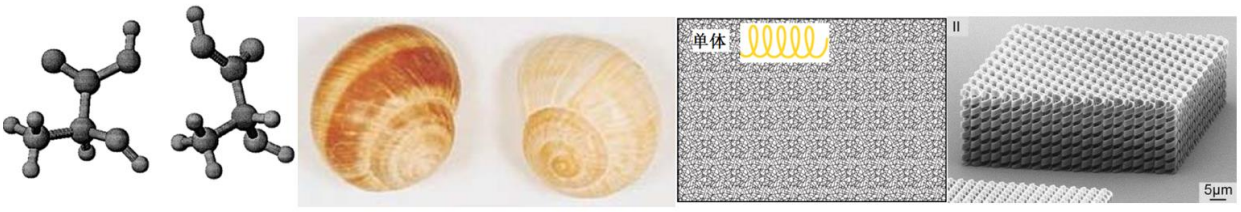

(a) (b) (c) (d)

Figure 2.7 The schematic diagram of chiral objects: (a) and (b) naturally existing whereas (c) and (d) artificially fabricated chiral bodies [55].

On the other hand, according to the size and spacing of chiral bodies, chiral materials can be divided into ordinary chiral materials and chiral metamaterials [51].

Metamaterials are artificial composite materials with exotic properties, which have attracted the intensive interest of physicists, material scientists, chemists and engineers over the past few decades [56]. Metamaterials comprise of periodically or randomly distributed artificial structures with size and spacing comparable with even smaller than the wavelength of interest [56, 57]. Using different designs, one can engineer material properties with unprecedented degrees of freedom and demonstrate extremely low-frequency plasmons [58], artificial magnetism [59] and negative refractive indices [60]. the early research just focused on metamaterials which can realize negative refractive indices, which promise numerous applications. In fact, the negative refraction with both negative permittivity and permeability was achieved by metamaterial. Metamaterial is concept was initially verified at microwave frequencies and then extended deeply into the visible regime [61, 62].

Belonging to a sort of metamaterials, chiral metamaterials exhibit many intriguing properties such as single negative refraction for one circularly polarized (RCP or LCP) component of light caused by strong chirality rather than double negative permittivity and permeability. Pendry had proposed a chiral metamaterial with single structure which realize negative refraction [35]. In addition, chiral metamaterials have attracted much interest because of their extremely strong optical activity [63, 64], which promises the ability to create compact broadband circular polarizers [65] and asymmetric transmission [66, 67].

As the example of applications, Figure 2.8 shows a schematic of a multi-hologram using a planar chiral metasurface with a planar chiral structure consisting of nanorods coated on a substrate with a thickness comparable to the lateral dimension. In fact, it gives the different response of the surface to the opposite circularly polarized light. Figure 2.8 (a) shows that when

the illumination of LCP light at normal incidence, the reconstructed 'flower' and the 'bee' are on the left side and on the right side of the incident beam, respectively. The two off-axis images are symmetrically distributed. The blue nanorods and purple nanorods represent the chiral metasurface holograms for 'flower' and 'bee', respectively.

When the relative position changed chiral metasurface may give opposite output as seen in Figure 2.9. This means that the chiral metasurface can be applied to the development of a new type of circularly polarization multiplexing function for switchable devices [69].

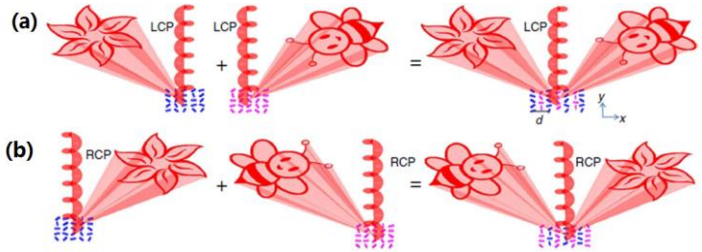

Figure 2.8 The schematic diagram of the generation of the multiplexed hologram based on meta-surface with the plane-chiral body [68].

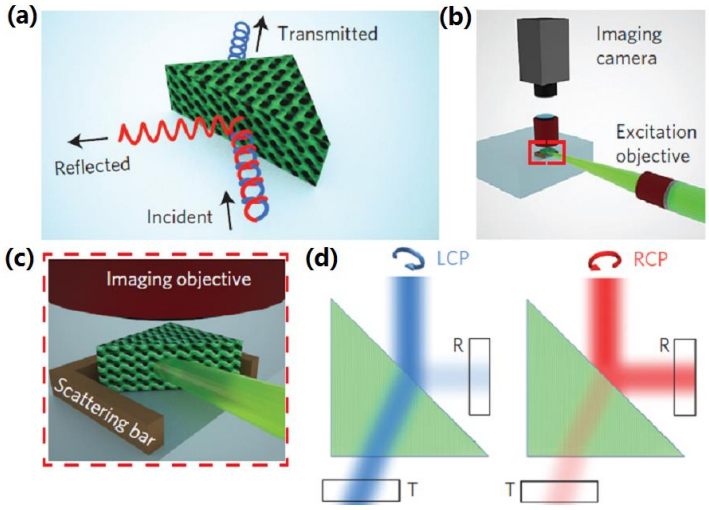

Figure 2.9 The schematic diagram of a beam splitter for circularly polarized light based on metamaterial with structural chirality [70].

2.2.2 Constitutive relations

Here we came back to show the concrete response of the ordinary chiral material namely, dielectrically chiral medium to the electromagnetic fields.

The chiral medium belongs to a class of electromagnetic (EM) materials that posses cross coupling between the electric field and magnetic field, which have promising prospects in the

engineering applications. The characteristic response of such materials can be specified by their constitutive relations which relate the electric displacement **D** and magnetic flux densities **B** to the electric field **E** and magnetic field **H**. If all the field vectors are linearly related, the medium is said to be linear one otherwise nonlinear one.

Actually, there several sets of constitutive relations suitable for describing the linear response of the medium to the electromagnetic fields, which were proposed by different scholars. We often meet the Born's, Tellegen's, Condon's and Post's constitutive relations with the form of

$$\begin{aligned}\mathbf{D} &= \varepsilon\left(\mathbf{E} + \xi_B \nabla \times \mathbf{E}\right) \\ \mathbf{B} &= \mu \mathbf{H}\end{aligned} \qquad \text{(Born's formulae)} \qquad (2.1)$$

where ξ_B is a chiral parameter linked with curl of the electric field that in fact, related to the magnetic field via Maxwell's curl equation for the relation between **E** and **B**. This relation are nonreciprocal, which does not satisfy critical angle of incidence when studying the transmission and reflection on the interface between chiral and achiral media. Therefore, the revised version had been proposed and developed by several persons like P. K. L. Drude, M. Born, F. I. Fedorov.

$$\begin{aligned}\mathbf{D} &= \varepsilon_{\mathrm{D}}\left(\mathbf{E} + \xi_{\mathrm{D}} \nabla \times \mathbf{E}\right) \\ \mathbf{B} &= \mu_{\mathrm{D}}\left(\mathbf{H} + \xi_{\mathrm{D}} \nabla \times \mathbf{H}\right)\end{aligned} \qquad \text{(Drude-Born-Fedorov's formulae)} \qquad (2.2)$$

where ξ_D is a chiral parameter, it can be related to the optical rotation δ of the medium via $\xi_D = -\omega^2 \varepsilon\mu = -\delta / k_0^2 n_0^2$.

Condon model is represented by the time domain and the time-harmonic as

$$\begin{aligned}\mathbf{D} &= \varepsilon_{\mathrm{C}}\mathbf{E} - \kappa \frac{\partial \mathbf{H}}{\partial t} \\ \mathbf{B} &= \mu_{\mathrm{C}}\mathbf{H} + \kappa \frac{\partial \mathbf{E}}{\partial t}\end{aligned} \qquad \text{(Condon's formulae)} \qquad (2.3)$$

where ε_{c} denotes dielectric constant under the Condon formalism $\varepsilon_{\mathrm{c}} = \varepsilon / (1 - \varepsilon\mu\omega^2\xi^2)$, μ_c represents permeability under the Condon model $\mu_C = \mu / (1 - \varepsilon\mu\omega^2\xi^2)$ and κ stands for chiral parameters under the Condon model $\kappa = \varepsilon\mu\xi / (1 - \varepsilon\mu\omega^2\xi^2)$.

Tellegen model is also discussed in the time domain as

$$\mathbf{D} = \varepsilon_{\mathrm{T}}\mathbf{E} - \zeta\frac{\partial \mathbf{H}}{\partial t}$$
$$\mathbf{B} = \mu_{\mathrm{T}}\mathbf{H} + \zeta\frac{\partial \mathbf{E}}{\partial t} \qquad \text{(Tellegen 's formulae)} \qquad (2.4)$$

where ε_T symbolizes dielectric constant under the Condon model $\varepsilon_T = \varepsilon/(1-\varepsilon\mu\omega^2\xi^2)$, μ_T denotes permeability under the Condon model $\mu_T = \mu/(1-\varepsilon\mu\omega^2\xi^2)$ and ζ stands for chiral parameters under the Condon model $\zeta = j\,\mu\varepsilon\omega\xi/(1-\mu\varepsilon\omega^2\xi^2)$.

Finally, the Post model in the electromagnetic properties of a homogeneous isotropic chiral medium may be described by the constitutive relations

$$\mathbf{D} = \varepsilon_P\mathbf{E} + j\xi_P\mathbf{B}$$
$$\mathbf{B} = \mu_P(\mathbf{H} - j\xi_P\mathbf{E}) \qquad \text{(Post's formulae)} \qquad (2.4)$$

Where ε_P symbolizes dielectric constant under the Condon model $\mu_p = \mu/(1-\mu\varepsilon\omega^2\beta^2)$, μ_P denotes permeability under the Condon model $\varepsilon_P = \varepsilon$ and ς stands for chiral parameters under the Condon model $\varsigma = \omega\varepsilon\xi$.

All the above mentioned equations are equivalent in the harmonic expression with factor of $\exp(-j\omega t)$, all parameters describing the chirality are also equivalent physically to characterize the electromagnetic coupling [71]. Substituting any set of the constitutive relations into the source-free and time-harmonic Maxwell's curl equations yield the same results for time-harmonic fields[72, 73]. Without loss of generality, in thesis, we will consider the Post constitutive relations combining with Maxwell's curl equations. However, the use of each relation has its advantages and disadvantages, for some specific research methods, select the appropriate constitutive relations will simplify the consideration of a problem.

2.3 Conventional chiral waveguide

A chiral waveguide is usually composed of chiral medium in core and/or cladding. The idea of adding chiral materials to waveguides had been proposed long years ago and many researchers studied different kinds of chiral waveguides [15].

In 1988, Bassiri S et al. studied the transmission through a interface with dielectric chiral media and through a chiral slab. The results were compared with previous data, and the physical equivalence of the results was demonstrated. He has obtained the total internal reflection angle

and Brewster's angle. The effects of the chirality on the polarization and the intensity of the reflected wave from the chiral half-space were discussed and illustrated by using the Stokes parameters. The propagation of electromagnetic waves through an infinite slab of chiral medium was formulated for oblique incidence and solved analytically for the case of normal incidence. It was shown that the plane of polarization of the transmitted wave is rotated with respect to that of the incident wave and that the plane of polarization of the reflected wave is unchanged with respect to that of the incident wave [74].

In 1989, Engheta et al. studied the propagation of electromagnetic waves in a cylindrical waveguides of arbitrary cross sectional shape and filled with a homogeneous, lossless, isotropic, chiral material, which is called chirowaveguides. They had validated that in these waveguides the individual TE, TM, or TEM modes cannot be supported. It has also been demonstrated that, owing to the chiral properties of the material inside the longitudinal components of fields are coupled. As an illustrative example the parallel-plate chirowaveguide is analyzed, and the corresponding dispersion relations and Brillouin diagrams were obtained. Some of the novel applications of chirowaveguides to optical directional couplers, photonic switches, and slow-wave structures have been presented [75].

In 1990, Svedin J developed the chiral finite element method for the study of transmission characteristics in chiral waveguides. He had concluded that with this method, it is possible to arbitrarily design the structure and material of the waveguide [76]. In the same year, Pelet P and Engheta N had analyzed the wave propagation and proposed the mode coupling theory for a cylindrical chirowaveguide filled with an isotropic chiral material [77]. In this study, it was assumed that the chiral strength was small enough to be considered as a perturbation. When considering the first two modes, the coupled equations can be solved by set of unperturbed solutions .

It is found that the periodic exchange of the energy between the modes in the waveguide is demonstrated and the coupling coefficient is proportional to the chiral parameter. When the phases are matched, the propagation constants of these two modes are equal, so that the energy can be completely converted from the TE to TM mode and vice versa. That means the mode conversion can be realized without employing materials which need biasing fields [77].

In 1995, Mahmoud S studied the guided mode by chiral column and flat open waveguide structures. It was found that the mode in the waveguide splits under the effect of chirality and

increases with the increase in chiral strength. The cutoff frequency is related to the rotation of each mode. If the chiral material is right-handed, it is possible that the guided mode in the high frequency region is a right-handed circular polarization mode [78]. This implies that the chirality provides a parameter for dispersion control of the waveguide. In the non-chiral waveguides, the structure and size of the waveguide are generally used to control the dispersion of the modes. For specific devices, size and structure of waveguide generally cannot make any significant changes, and their effects are only applied on the dispersion medium. The refractive index and dispersion are related to the absorption of the material, so it can be difficult to significantly change the mode dispersion without changing the mode loss. Theoretical studies have shown that it is possible to obtain a large change in mode dispersion by introducing very weak chiral strength in the waveguide. This is due to the fact that the effect of chirality on the dispersion of the overall pattern can be manifested by the effective refractive index of the material itself. The extremely weak chiral strength does not substantially change the absorption characteristics of the waveguide. Chiral waveguides may be developed as directional couplers with better performance and optical energy transfer between different channels [77]. In addition, some scholars have found that chiral waveguides can be used as mode converters to achieve TE/TM conversion fields [15].

In 2011, Dong J et al. have been investigated theoretically the characteristics of guided and surface wave modes in the four-layer slab waveguide containing chiral nihility core. The characteristic equation of guided modes was obtained. Effects of chirality parameter on dispersion curves, energy flux distribution and power were examined and some peculiar features were found, for examples, the existence of fundamental mode for all chirality parameters, the existence of surface wave mode for smaller and larger chirality parameters, abnormal dispersion curves with different shape, positive energy flux in the chiral nihility core, and zero power at some normalized frequencies. The feature is different from that in four-layer slab waveguide with left-handed material. Guided modes in the chiral nihility waveguide are not TE or TM modes, they are hybrid modes and have both TE and TM components. The results have potential applications in novel waveguide devices such as directional couplers, high efficient waveguide sensors.

2.4 Dielectrically chiral fiber

Dielectrically chiral optical fiber is a new type of cylindrical chiro-wave guides filed with homogeneous isotropic chiral medium. In 1994, Qiu R et al. studied the chiral fiber and a traditional fiber with chiral structure. The equations for the field distribution and dispersion of the fiber mode were deduced, and the chiral intensity for mode dispersion was analyzed in detail[79]. In the same year, Singh A et al. studied the mode cutoff problem of chiral fiber. Both the fiber core and the cladding are chiral, but the chirality strength is different. They derived the analytical solution of the cutoff condition, which is the same as that of a non-chiral optical fiber. The chirality of the cladding would cause a cut-off condition similar to that of achiral fiber. The cutoff conditions of the standard criteria for the chiral step-index fiber will be split into two cutoff conditions; only when the cladding contains chirality, the energy in the core will gradually decrease [80].

In 1995, Mahmoud S pointed out that when the core and cladding impedance are consistent, the modes of the circular optical fiber under the weak conduction approximation are left-handed and right-handed circularly polarized (LCP and RCP) [78]. In 2002, Janeiro F et al. studied the more general chiral optical fibers in which the core and the cladding are filled with homogeneous chiral media, and pointed out the possibility of the semi-leaky mode [81].

In 2004, Li J. et al. studied self-induced optical rotation in nonlinear chiral fiber based on the theory of nonlinear optical transmission. They established generalized nonlinear Schrödinger equation (GNLSE) and discussed the mechanism for formation of the chiral Soliton for both LCP and RCP components and the applications in all-optical switching [82].

In 2010, Argyros A. proposed the most suitable material for the preparation of chiral optical single-core single-mode (SCSM) fiber like polymer, because the polymer is not easy to dope with other chiral organic molecules, but also can be polymerized with a chiral group of molecules [83]. In the same year, Deng J. studied guided and surface modes in the chiral nihility fiber consisting of a chiral nihility metamaterial core with an achiral cladding have been investigated[84]. The fiber is composed of the chiral nihility super material core and the non-chiral cladding. The dispersion equations of guided and surface modes in the chiral nihility fiber and their cutoff frequencies are derived. Dispersion curves of guided and surface modes are presented and the effect of chirality parameter on dispersion curves is discussed in detail. Some novel propagation characteristics are found such as.

In 2011, Y Li and J Cao developed the model theory of chiral optical fiber, in which both the cladding and core are chiral media. They pointed out that the chiral fiber plays an important role in the wave impedance. Their analytical and numerical results demonstrated that the proper design of the optical fiber cladding and the chirality in the core can support the circular polarized mode, they affect dispersion in different ways [85].

In 2013, Cao Y. et al. studied the chiral multilayer Bragg mode splitting in optical fiber, in the case of chirality, the degenerate mode in the case of chiral splitting occurs, and the numerical calculation shows that the fiber can selectively support the rotation of the circular polarization modes of different wavelengths [86].

In 2014, Cao Y and Li J. theoretically studied the transverse field distribution of chiral negative refractive optical fiber that guides transverse electromagnetic modes. In their report, they include arbitrariness of modal field and arbitrarily scalable core radius. Based on these novel properties, they conceptually proposed a new type of space-division multiplexing that uses different spatial positions of the core of such fascinating fibers as different data paths [87].

As a kind of new material fiber, the research of chiral optical fiber has many advantages compared with the conventional optical fiber. For example, depending on the mode, the different polarized light carries different information, which may double the fiber transmission bandwidth but not increase the transmission window too much. Therefore, based on the consideration of new material and new structured optical fiber, the researchers put forward on the dielectrically chiral fiber and nonlinear fiber couplers.

2.5 Chiral effects in nonlinear optics

Nonlinear optics (NLO) has been recognized for several years as a field of research with important applications in optoelectronic techniques[88]. Much work has been devoted in searching and characterizing the suitable materials with excellent performance. In 1980s it became clear that organic materials (especially polymers) could be used in second- and third-order nonlinear processes [15]. Among various classes of optical materials, the chiral material structure has received renewed attention as an important class of materials for NLO applications. For examples, third-order NLO effects in optically active liquids, Kerr optical rotatory dispersion (ORD) and Kerr circular dichroism (CD) effects, have been studied in chiral molecular systems, and the microscopic expression for the Kerr CD has been obtained .

Even-order nonlinear optical processes are forbidden, in the electric-dipole approximation, in material systems that possess a center of symmetry [89, 90]. The present challenge in materials development for second-order nonlinear optics is therefore to find noncentrosymmetric molecules that have a large molecular hyperpoiarizability and that can be organized in a noncentrosymmetric macroscopic arrangement to give rise to a non-vanishing second-order susceptibility. On the other hand, symmetry properties of magnetic-dipole and electric-quadrupole transitions are different from those of electric-dipole transitions. For example, even-order processes involving a single magnetic-dipole or electric-quadrupole transition in place of one of the electric-dipole transitions can be allowed in cases in which pure electric-dipole nonlinearities are forbidden [89, 91].

Chiral materials are particularly interesting in nonlinear optical applications due to two different aspects. First, their molecular structure is necessarily noncentrosymmetric and consequently, certain even-order nonlinearities become electric-dipole allowed in highly symmetric macroscopic samples [88, 91]. Second, magnetic-dipole transitions of chiral molecules can be very strong with strengths up to ~ 20 % of those of electric-dipole transitions [88, 91]. For example, second harmonic generation involving magnetic-dipole transitions from a racemic and centrosymmetric crystal of chiral molecules has been observed [91].

Chiral media possess unique nonlinear optical properties. In 2004, Robert W Boyd et al. studied chirality and polarization effects in nonlinear optics. It has been pointed out that polarization effects play an even more important role in nonlinear optics than in linear optics because of the richer set of phenomena describable by higher-order tensor relations [90]. In this regards, the research on polarization aspects of nonlinear optical interactions has been paid special attention in nonlinear optical interactions of chiral isotropic materials.

The importance of nonlinear effects may be reflected in some nonlinear processes in bulk chiral medium and its film such as second-order nonlinear optical processes, including the second harmonic generation (SHG) [92, 93], and sum or difference frequency generation (SFG or DFG), electro-optic effect (EO), optical rectification (OR), even in some higher order nonlinear processes like Kerr effects, including the self-phase modulation (SPM) and cross phase modulation (XPM). It is obvious that most of the current studies concerned to nonlinear chiral medium and its film are mainly focused on the second-order nonlinear processes rather than the third order ones, for instance, the Kerr effects [94, 95]. Nonlinear optical activity including

nonlinear CB and nonlinear CD also exists in the processes [89].

Nonlinear effects in chiral optical fibers may occur due to (1) change in the refractive index of the medium with optical intensity and, (2) inelastic scattering phenomenon. The power dependence of the refractive index is responsible for the Kerr-effect. Depending upon the type of input signal, the Kerr-nonlinearity manifests itself in three different effects such as SPM, XPM and four-wave mixing (FWM). At high power level, the inelastic scattering phenomenon can induce stimulated effects such as stimulated Brillouin scattering (SBS) and stimulated Raman scattering (SRS). The intensity of scattered light grows drastically if the incident power exceeds a certain threshold.

In, 2003 Torres-Silva H et al. studied chiral effects on optical solitons and. We should point out that they started from Drud-Born-Fedorov constitutive relation (equivalent to Post's formalism) derived generalized chiral nonlinear Schrodinger equation (NLSE) and also discussed some simplified situations for the generalized NLSE with considering the Kerr nonlinearity [96]. In their work, they had not included the optical rectification (OR) effect that occurs and may make contribution similar to Kerr effect as we see in the chapter two.

They discussed its simplified form, but they were just started from the, and only consider the Kerr nonlinearity.

Jun-Qing Li et al. studied self-induced optical rotation of soliton in chiral fiber [82] starting from Maxwell's equations and macroscopic polarization. They obtained nonlinear Schrödinger equation (NLSE) which can describe the propagation of strong light in anisotropic chiral fiber with weak special dispersion for LCP and RCP polarized components in chiral fiber and discussed some simplified cases [97].

In 2015, Zinelabiddine M et al. studied on chiroptical fiber nonlinearities with new formulation of constitutive equations. They theoretical presented light pulse propagating in a chiroptical fiber by considering Kerr effect in their work. The results obtained in this study indicates that nonlinear chirality parameter becomes the key factor to estimate chiroptical fiber dispersion and nonlinearity [98].

More recently, Zinelabiddine M et al. considered modeling of a light pulse in bi-isotropic optical fiber with Kerr effect using the Tellegen constitutive relation. The two constitutive equations approach for nonlinear bi-isotropic media were proposed to highlight nonlinear effect, which is due to the magnetization vector under the influence of a strong electric field [99]. The

nonlinear parameter of magnetization vector was illustrated, which is the important factors to estimate bi-isotropic optical fiber dispersion and nonlinearity. They have used split-step Fourier (SSF) method for the simulation and solved the nonlinear Schrödinger equation (NLSE) [99].

In optical communication devices, nonlinear polarization-dependent effects are also of interest [100]. In this dissertation, we consider second-order and third order nonlinear responses to establish chiral fiber waveguide as one of the new candidates. As a result, chiral media may find applications in optic communication such as a waveguide, fiber and derivative devices [15], polarization mode converters and all-optical switches, optical sensors and integrated optics devices [15]. Also in the recent years, chiral materials have attracted much attention because the negative refractive index can be realized in [101].

2.6 Research Status on Nonlinear Chiral fiber couplers

To meet the demands of high-power fiber lasers, a new fiber structure named chirally coupled core (CCC) fiber has concerned the attention of researchers all over the world. In fact, CCC fiber consists of two cores, one of which is a central core distributed along the axial direction, and the other is a side core that is offset from the central axis as illustrated in Figure 1.1. The unique structure results in advantages of robust single-mode performance, mode-distortion-free splicing and compact coiling of CCC fiber. Based on a brief description of the theory about CCC fiber, this research focuses on the research progress and application prospect of CCC fiber [34].

As one of the candidates of information distributors that of very vital in modern optical networks, the nonlinear fiber coupler controlled by light gradually become one of the basic components in all-optical fiber communication systems since proposed in the early 1980's by Jensen [1]. Intense light can change the portion of the distributed optical information among output ports by nonlinear effect, which is, in fact, forms a family of all-optical switches [2]. The nonlinear fiber couplers and its application have been presented systematically by Govind P. Agrawal [3, 4].

It should be pointed out that most of the fiber couplers, which are constructed by the ordinary symmetric materials, like silica-based fiber (SiO_2) [4] have been studied completely and become available commercially. However, there still exist some problems, such as the linear and nonlinear coupling in the chiral fiber couplers and the performance of corresponding devices. So

it is very necessary to do research on nonlinear coupling characteristics in chiral fibers.

In this research, the recent advances in CCC fiber are reviewed along with the introduction of its basic structure and related parameters. Meanwhile, the special functions of the CCC structure are expounded from three aspects, and the coupling between the higher-order modes in the fiber is discussed from the quasi-phase matching condition.

straight core, coupling the high order mode into the side core and producing high loss to it. The base modes [26, 27] in the central core can be transmitted almost without loss. In this way, the CCC fiber [28–33] does not rely on any mode control technology to maintain a single-mode transmission while achieving a large mode field area. Moreover, the above problems are well solved. The reason why CCC can achieve stable single-mode transmission in the case of large core diameter is the special helical structure of its side core [34, 35]. The composite structure of the new type of fiber in which the side cores spiral around the central core can achieve the following three functions.

In 2007, Liu et al. from the University of Michigan [38, 39] proposed the concept of CCC fiber and confirmed that CCC fiber is equivalent to standard single-mode fiber with single mode transmission characteristics. In order to further verify the simulation results, Liu et al. [40] prepared CCC fiber with a central core diameter of 35 μm and a side core diameter of 12 μm. And the fundamental mode loss of the fiber is 0.095 dB/m. It is transmitted in the core with near lossless. This is the first demonstration of the stable single-mode transmission characteristics of CCC fiber. In 2008, the lab produced an ytterbium-doped double-clad CCC fiber. Among them, the central core diameter is 33 μm and the numerical aperture is 0.06. The side core diameter is 16 μm and the numerical aperture is 0.1. The side-core helix pitch Λ is 7.4 mm, and the edge-to-edge distance between the two cores is 4 μm. In experiments, the active fiber was pumped with a 915 nm laser diode and a 37 W laser output was obtained at 1066 nm. The slope efficiency is 75% and the output spot confirms the fundamental mode. This experiment further verifies the superiority of the CCC fiber, indicating that the fiber can be used as the gain medium of the laser like ordinary fiber. The formed fiber laser has the advantages of high slope efficiency and low threshold power, and the output beam quality has been greatly improved compared with large mode area fiber.

In 2009, Huang et al. from the University of Michigan [41] demonstrated single-mode power scaling in fiber laser systems built using 35 μm core Yb-doped double-clad CCC fiber.

Output power up to 250 W is demonstrated in their study with pulse width of 10 ns and the pulse energy of 1.14 mJ. The peak power is 114 kW and the amplification slope efficiency reaches 74%. Also, the system output spot is single mode. In 2010, the team applied CCC fiber in a master oscillator power amplifier (MOPA) structure to increase the system output power. In the experiment, a 2.7 m long air-clad Ytterbium-doped CCC fiber was used as the gain medium of the power amplifier. The fiber was excited with 2.2 W signal light and the MOPA structure power output of 511 W was achieved. The amplifier slope efficiency is 70% [42–44]. In 2011, Ma et al. [22] established a new reference frame from optical angular momentum by using Maxwell equations and finite element method. A complete theoretical analysis of the mode effects in the CCC fiber is obtained, and the mode matching conditions of the fiber are obtained. This is also the theoretical basis for the first disclosed CCC fiber. The theoretical basis of CCC fiber has been introduced in the previous article and will not be described here.

The University of Michigan Center for Ultrafast Optics, Sosnowski et al. [45, 46] used CCC fibers to conduct experiments with high average power and high peak power, respectively. The experimental setup for high average power is as follows: The system front end consisted of a 0.5 W 1.06 μm wavelength pulsed diode seed source, a CCC fiber preamplifier and a CCC fiber final stage amplifier. The final amplifier fiber assembly consisted of both Yb-doped and passive 33 μm core, 250 μm clad CCC fibers with a 0.46 NA cladding. The maximum output power achieved is 257 W at 338 W of pump power for a net optical-to-optical efficiency of 76% [47, 48].

In general, CCC has many advantages, which not only overcomes the disadvantage of weak guide fiber with great bending loss, but also realize stable single-mode transmission without any mode control technology. A series of related experiments also confirmed that CCC fiber has the advantages of high output power, high slope efficiency and good polarization-maintaining characteristics, which provides an effective way to increase the power of high-power fiber lasers and is conducive to the integrated development of laser systems [73]. In addition, the CCC fiber structure can also control nonlinear effects to realize special functions such as quantum communication [74]. It is certain that the CCC fiber has very important significance and broad development prospects in both scientific research and practical applications.

3. Theoretical Framework of Nonlinear Chiral Fiber Couplers

3.1 Introduction

In this chapter, we try to establish a theoretical framework describing the transmission of light through chiral nonlinear fiber couplers, whose structure has illustrated in Figure 1.1 assuming that light propagates along the z-direction.

Considering Post's constitutive relations and Maxwell's equations, we will make an attempt to obtain the generalized coupled chiral nonlinear Schrödinger equations (GCCNLSEs), based on which the evolution of LCP and RCP components in the fiber couplers can be discussed and the role of chirality in regulating the behavior of coupling and switching among different components will be demonstrated .

3.2 Coupling equations in chiral fiber couplers

In order to establish the coupled equations between two cores of chiral fiber coupler, both RCP and LCP components must be considered simultaneously. Using Maxwell's equations without free charge and current, and the Post's constitutive relations [77, 102] which can be written as

$$\begin{aligned} \mathbf{D} &= \varepsilon \mathbf{E} + j\xi_{\mathrm{C}} \mathbf{B} \\ \mathbf{H} &= j\xi_{\mathrm{C}} \mathbf{E} + 1/\mu \mathbf{B} \end{aligned}, \tag{3.1}$$

where $\mathbf{E}$ and $\mathbf{H}$ denote electric and magnetic field strength, $\mathbf{D}$ and $\mathbf{B}$ represent the electric and magnetic displacements, respectively. While $\varepsilon = \varepsilon_0 \varepsilon_r$, $\mu = \mu_0 \mu_r$ and ξ_c indicate the permittivity, permeability, and chiral admittance of the chiral medium, respectively. The chiral Helmholtz equation in time domain can also be obtained

$$\nabla \times \nabla \times \mathbf{E} + \mu_0 \varepsilon \frac{\partial^2}{\partial t^2} \mathbf{E} - j2\mu\xi_c \frac{\partial}{\partial t} \nabla \times \mathbf{E} = 0 \tag{3.2}$$

According to the coupled mode theory [103, 104], in the coupling region, the total optical field of the two waveguide in the time domain can be written as

$$\mathbf{E}(\mathbf{r}, t) = \mathbf{E}_1(\mathbf{r}, t) + \mathbf{E}_2(\mathbf{r}, t) \tag{3.3}$$

where the subscript 1 and 2 correspond to the different waveguide.

By considering the mode distribution and polarized components, the fields propagating along z-direction can be expressed as

$$\mathbf{E}_1(z,t) = \mathbf{e}_+ A_{1+}(z,t)F_{1+}(x,y)\exp(j\beta_{1+}z) + \mathbf{e}_- A_{1-}(z,t)F_{1-}(x,y)\exp(j\beta_{1-}z) \quad (3.4a)$$

$$\mathbf{E}_2(z,t) = \mathbf{e}_+ A_{2+}(z,t)F_{2+}(x,y)\exp(j\beta_{2+}z) + \mathbf{e}_- A_{2-}(z,t)F_{2-}(x,y)\exp(j\beta_{2-}z) \quad (3.4b)$$

where x and y denote orthogonal coordinates in the cross-sectional region of the waveguides and $\pm$ stands for RCP and LCP components and the polarization unit vectors ($\mathbf{e}_\pm$). The two eigenvectors $\mathbf{e}_\pm$ can be expressed as $\mathbf{e}_\pm = \sqrt{2}(\mathbf{e}_x \mp j\mathbf{e}_y)/2$ for the LCP and RCP components with an orthogonality of $\mathbf{e}_\pm \cdot \mathbf{e}_\pm = 0$, $\mathbf{e}_\pm \cdot \mathbf{e}_\mp = 1$ and $\mathbf{e}_\pm \times \mathbf{e}_\mp = \mp j\mathbf{e}_z$, where x and y denote orthogonal coordinates in the cross-sectional direction of the waveguides. In the equations, $A_{1,2\pm}(z,t)$, $F_{1,2\pm}(x,y)$ and $\beta_{1,2\pm}$ represent amplitudes, mode distributions and propagation constants in the chiral fiber couplers.

After some mathematical procedures one can get corresponding Helmholtz equation in frequency domain for nonmagnetic case

$$\nabla^2\tilde{\mathbf{E}}(\mathrm{r},\omega) + 2\omega\mu_0\xi_c\nabla\times\tilde{\mathbf{E}}(\mathrm{r},\omega) + n^2k_0^2\tilde{\mathbf{E}}(\mathrm{r},\omega) = 0 \quad (3.5)$$

where $k_0 = 2\pi/\lambda_0$ and λ_0 indicates a vacuum wavelength and $n = \sqrt{\varepsilon_r\mu_r}$ stands for the refractive index of the core.

From the coupled mode theory [103, 104], in the coupling region, the total optical field in the frequency domain can be divided into two parts

$$\tilde{\mathbf{E}}(z,\omega) = \tilde{\mathbf{E}}_1(z,\omega) + \tilde{\mathbf{E}}_2(z,\omega) \quad (3.6)$$

with

$$\tilde{\mathbf{E}}_1(z,\omega) = \tilde{A}_{1+}(z,\omega)F_{1+}(x,y)\mathbf{e}_+\exp(j\beta_{1+}z) + F_{1-}(x,y)\tilde{A}_{1-}(z,\omega)\mathbf{e}_-\exp(j\beta_{1-}z) \quad (3.6a)$$

$$\tilde{\mathbf{E}}_2(z,\omega) = \tilde{A}_{2+}(z,\omega)F_{2+}(x,y)\mathbf{e}_+\exp(j\beta_{2+}z) + \tilde{A}_{2-}(z,\omega)F_{2-}(x,y)\mathbf{e}_-\exp(j\beta_{2-}z) \quad (3.6b)$$

where $\tilde{A}_{1,2\pm}$ corresponds to the frequency components of the longitudinal amplitudes of the electric field for both polarizations in the frequency domain.

By substituting Eq. (3.6) into Eq. (3.5), we have the expressions for $\nabla\tilde{\mathbf{E}}(z,\omega)$, $\nabla\times\tilde{\mathbf{E}}(z,\omega)$ and $n^2k_0^2\tilde{\mathbf{E}}(\mathrm{r},\omega)$ as follows

$$\begin{aligned}\nabla\tilde{\mathbf{E}}(z,\omega)=&\left(\frac{\partial^2 F_{1+}}{\partial x^2}+\frac{\partial^2 F_{1+}}{\partial y^2}+j2\beta_{1+}F_{1+}\frac{\partial}{\partial z}-\beta_{1+}^2F_{1+}\right)\tilde{A}_{1+}\mathbf{e}_+\exp(j\beta_{1+}z)\\&+\left(\frac{\partial^2 F_{1-}}{\partial x^2}+\frac{\partial^2 F_{1-}}{\partial y^2}+j2\beta_{1-}F_{1-}\frac{\partial}{\partial z}-\beta_{1-}^2F_{1-}\right)\tilde{A}_{1-}\mathbf{e}_-\exp(j\beta_{1-}z)\\&+\left(\frac{\partial^2 F_{2+}}{\partial x^2}+\frac{\partial^2 F_{2+}}{\partial y^2}+j2\beta_{2+}F_{2+}\frac{\partial}{\partial z}-\beta_{2+}^2F_{2+}\right)\tilde{A}_{2+}\mathbf{e}_+\exp(j\beta_{2+}z)\\&+\left(\frac{\partial^2 F_{2-}}{\partial x^2}+\frac{\partial^2 F_{2-}}{\partial y^2}+j2\beta_{2-}F_{2-}\frac{\partial}{\partial z}-\beta_{2-}^2F_{2-}\right)\tilde{A}_{2-}\mathbf{e}_-\exp(j\beta_{2-}z)\end{aligned}\tag{3.7}$$

$$\begin{aligned}\nabla\times\tilde{\mathbf{E}}(z,\omega)=&-\beta_{1+}F_{1+}\tilde{A}_{1+}\mathbf{e}_+\exp(j\beta_{1+}z)-\beta_{1-}F_{1-}\tilde{A}_{1-}\mathbf{e}_-\exp(j\beta_{1-}z)\\&-\beta_{2+}F_{2+}\tilde{A}_{2+}\mathbf{e}_+\exp(j\beta_{2+}z)-\beta_{2-}F_{2-}\tilde{A}_{2-}\mathbf{e}_-\exp(j\beta_{2-}z)\end{aligned}\tag{3.8}$$

and

$$n^2k_0^2\tilde{\mathbf{E}}(z,\omega)=k_0^2n^2(\tilde{\mathbf{E}}_1(z,\omega)+\tilde{\mathbf{E}}_2(z,\omega))\tag{3.9}$$

Here we introduce Kerr effect into the fiber, thus

$$n=n_{0\pm}+n_{2\pm}\left|\tilde{\mathbf{E}}(z,\omega)\right|^2\tag{3.10}$$

where $n_{0\pm}$ and $n_{2\pm}$ denote the linear and nonlinear coefficient of refractive index for RCP and LCP components, respectively. In order to simplify our discussion, we assume that there is no difference in the coefficients of the nonlinear refractive index for RCP and LCP components, namely $n_{2+}=n_{2-}=n_2$. It should be pointed out that the nonlinearity is so weak that it can be treated as a perturbation. That is to say, the nonlinear phenomenon is a weak effect compared with the main behavior of linear effect.

By substituting Eqs. (3.6), (3.7), (3.8) and (3.9 into (3.5), considering perturbation assumption and collecting the terms with the same polarization and separating of variables, one can obtain the set of equations for the modes as

$$\frac{\partial^2 F_{1+}}{\partial x^2}+\frac{\partial^2 F_{1+}}{\partial y^2}+k_0^2\left[(n_+^2-n_{0+}^2)-\bar{\beta}_{1+}^2\right]F_{1+}=0\tag{3.11a}$$

$$\frac{\partial^2 F_{1-}}{\partial x^2}+\frac{\partial^2 F_{1-}}{\partial y^2}+k_0^2\left[(n_-^2-n_{0-}^2)-\bar{\beta}_{1-}^2\right]F_{1-}=0\tag{3.11b}$$

$$\frac{\partial^2 F_{2+}}{\partial x^2}+\frac{\partial^2 F_{2+}}{\partial y^2}+k_0^2\left[(n_+^2-n_{0+}^2)-\bar{\beta}_{2+}^2\right]F_{2+}=0\tag{3.11c}$$

$$\frac{\partial^2 F_{2-}}{\partial x^2}+\frac{\partial^2 F_{2-}}{\partial y^2}+k_0^2\left[(n_-^2-n_{0-}^2)-\bar{\beta}_{2-}^2\right]F_{2-}=0 \tag{3.11d}$$

and equations for the amplitudes as

$$j2\beta_{1+}\frac{\partial A_{1+}}{\partial z}+(\bar{\beta}_{1+}^2-\beta_{1+}^2)A_{1+}-2\omega\mu\xi_c\beta_{1+}A_{1+}=0 \tag{3.12a}$$

$$j2\beta_{1-}\frac{\partial A_{1-}}{\partial z}+(\bar{\beta}_{1-}^2-\beta_{1-}^2)A_{1-}-2\omega\mu\xi_c\beta_{1-}A_{1-}=0 \tag{3.12b}$$

$$j2\beta_{2+}\frac{\partial A_{2+}}{\partial z}+(\bar{\beta}_{2+}^2-\beta_{2+}^2)A_{2+}-2\omega\mu\xi_c\beta_{2+}A_{2+}=0 \tag{3.12c}$$

$$j2\beta_{2-}\frac{\partial A_{2-}}{\partial z}+(\bar{\beta}_{2-}^2-\beta_{2-}^2)A_{2-}-2\omega\mu\xi_c\beta_{2-}A_{2-}=0 \tag{3.12d}$$

The amplitudes $A_{1\pm}$ and $A_{2\pm}$ vary along the coupler length because of the energy exchange of the modes. To find how they evolve with z, we multiply Eqs. (3.12a), (3.12b), (3.12c) and (3.12d) by F_{1+}^*, F_{1-}^*, F_{2+}^* and F_{2-}^* respectively, use Eq. (3.11) and integrate over the entire x-y plane. This procedure leads to the following set of four coupled-mode equations in the frequency domain:

$$\begin{aligned}j\frac{\partial\tilde{A}_{1+}}{\partial z}+(\bar{\beta}_{1+}-\beta_{1+})\tilde{A}_{1+}-\omega\mu\xi_c\tilde{A}_{1+}+\frac{k_0^2 n_{0\pm}n_2}{\beta_{1+}}\tilde{A}_{1+}\int\int_{-\infty}^{+\infty}|\tilde{\mathbf{E}}|^2\,F_{1+}F_{1+}^*dxdy\\+\frac{k_0^2 n_{0\pm}n_2}{\beta_{1+}}\tilde{A}_{2+}\int\int_{-\infty}^{+\infty}|\tilde{\mathbf{E}}|^2\,F_{2+}F_{1+}^*dxdy=0\end{aligned} \tag{3.13a}$$

$$\begin{aligned}j\frac{\partial\tilde{A}_{1-}}{\partial z}+(\bar{\beta}_{1-}-\beta_{1-})\tilde{A}_{1-}-\omega\mu\xi_c\tilde{A}_{1-}+\frac{k_0^2 n_{0-}n_2}{\beta_{1-}}\tilde{A}_{1-}\int\int_{-\infty}^{+\infty}|\tilde{\mathbf{E}}|^2\,F_{1-}F_{1-}^*dxdy\\+\frac{k_0^2 n_{0-}n_2}{\beta_{1-}}\tilde{A}_{2-}\int\int_{-\infty}^{+\infty}|\tilde{\mathbf{E}}|^2\,F_{2-}F_{1-}^*dxdy=0\end{aligned} \tag{3.13b}$$

$$\begin{aligned}j\frac{\partial\tilde{A}_{2+}}{\partial z}+(\bar{\beta}_{2+}-\beta_{2+})\tilde{A}_{2+}-\omega\mu\xi_c\tilde{A}_{2+}+\frac{k_0^2 n_{0+}n_2}{\beta_{2+}}\tilde{A}_{1+}\int\int_{-\infty}^{+\infty}|\tilde{\mathbf{E}}|^2\,F_{2+}F_{2+}^*dxdy\\+\frac{k_0^2 n_{0+}n_2}{\beta_{2+}}\tilde{A}_{2+}\int\int_{-\infty}^{+\infty}|\tilde{\mathbf{E}}|^2\,F_{1+}F_{2+}^*dxdy=0\end{aligned} \tag{3.13c}$$

$$\begin{aligned}j\frac{\partial\tilde{A}_{2-}}{\partial z}+(\bar{\beta}_{2-}-\beta_{2-})\tilde{A}_{2-}-\omega\mu\xi_c\tilde{A}_{2-}+\frac{k_0^2 n_{0-}n_2}{\beta_{2-}}\tilde{A}_{1-}\int\int_{-\infty}^{+\infty}|\tilde{\mathbf{E}}|^2\,F_{2-}F_{2-}^*dxdy\\+\frac{k_0^2 n_{0+}n_2}{\beta_{2-}}\tilde{A}_{2-}\int\int_{-\infty}^{+\infty}|\tilde{\mathbf{E}}|^2\,F_{1-}F_{2-}^*dxdy=0\end{aligned} \tag{3.13d}$$

where $\left|\tilde{\mathbf{E}}\right|^2 = \left(\tilde{\mathbf{E}}_1 + \tilde{\mathbf{E}}_2\right)\cdot\left(\tilde{\mathbf{E}}_1 + \tilde{\mathbf{E}}_2\right)^*$ is proportional to the intensity of the total electric field which can be expressed by

$$\begin{aligned}|\tilde{\mathbf{E}}|^2 = &\left|\tilde{A}_{1+}\right|^2\left|F_{1+}\right|^2 + \left|\tilde{A}_{1-}\right|^2\left|F_{1-}\right|^2 + \left|\tilde{A}_{2+}\right|^2\left|F_{2+}\right|^2 + \left|\tilde{A}_{2-}\right|^2\left|F_{2-}\right|^2 \\ &+ \tilde{A}_{1+}\tilde{A}_{2+}^* F_{1+}F_{2+}^* + \tilde{A}_{1-}\tilde{A}_{2-}^* F_{1-}F_{2-}^* + \tilde{A}_{2+}\tilde{A}_{1+}^* F_{2+}F_{1+}^* + \tilde{A}_{2-}\tilde{A}_{1-}^* F_{2-}F_{1-}^*\end{aligned} \tag{3.14}$$

here, the last four terms in the right hand side of Eq. (4-14) are associated with the effect of wave mixing. In fact, the process of wave mixing needs phase matching conditions[94], which is not satisfied for the fiber with ordinary structure. Thus, the last term may be ignored in our case. Thus, Eq. (4-13) can be more simplified to

$$j\frac{\partial\tilde{A}_{1+}}{\partial z} + (\bar{\beta}_{1+} - \beta_{1+})\tilde{A}_{1+} - \omega\mu\xi_c\tilde{A}_{1+} + \Delta\tilde{\beta}_{1+}\tilde{A}_{1+} + \kappa_{1+2}\tilde{A}_{2+} + \kappa_{1+2-}\tilde{A}_{2-} = 0 \tag{3.15a}$$

$$j\frac{\partial\tilde{A}_{1-}}{\partial z} + (\bar{\beta}_{1-} - \beta_{1-})\tilde{A}_{1-} - \omega\mu\xi_c\tilde{A}_{1-} + \Delta\tilde{\beta}_{1-}\tilde{A}_{1-} + \kappa_{1-2-}\tilde{A}_{2-} + \kappa_{1-2+}\tilde{A}_{2+} = 0 \tag{3.15b}$$

$$j\frac{\partial\tilde{A}_{2+}}{\partial z} + (\bar{\beta}_{2+} - \beta_{2+})\tilde{A}_{2+} - \omega\mu\xi_c\tilde{A}_{2+} + \Delta\tilde{\beta}_{2+}\tilde{A}_{1+} + \kappa_{2+1+}\tilde{A}_{1+} + \kappa_{2+1-}\tilde{A}_{1-} = 0 \tag{3.15c}$$

$$j\frac{\partial\tilde{A}_{2-}}{\partial z} + (\bar{\beta}_{2-} - \beta_{2-})\tilde{A}_{2-} - \omega\mu\xi_c\tilde{A}_{2-} + \Delta\tilde{\beta}_{2-}\tilde{A}_{1-} + \kappa_{2-1-}\tilde{A}_{1-} + \kappa_{2-1+}\tilde{A}_{1+} = 0 \tag{3.15d}$$

where $\Delta\tilde{\beta}_{i\pm}\ (i=1,2)$ represents the nonlinear contribution and $\kappa_{1\pm2\pm}$, $\kappa_{1\pm2\mp}$, $\kappa_{2\pm1\pm}$ and $\kappa_{2\pm1\mp}$ correspond to the coupling coefficients, which can be given as

$$\Delta\tilde{\beta}_{1+} = \frac{k_0^2 n_{0+} n_2}{\beta_{1+}}\int_{-\infty}^{+\infty}\int(\left|\tilde{A}_{1+}\right|^2\left|F_{1+}\right|^4 + \left|\tilde{A}_{1-}\right|^2\left|F_{1-}\right|^2 F_{1+}F_{1+}^*)dxdy \tag{3.16a}$$

$$\Delta\tilde{\beta}_{1-} = \frac{k_0^2 n_{0-} n_2}{\beta_{1-}}\int_{-\infty}^{+\infty}\int(\left|\tilde{A}_{1-}\right|^2\left|F_{1-}\right|^4 + \left|\tilde{A}_{1+}\right|^2\left|F_{1+}\right|^2 F_{1-}F_{1-}^*)dxdy \tag{3.16b}$$

$$\Delta\tilde{\beta}_{2+} = \frac{k_0^2 n_{0+} n_2}{\beta_{2+}}\int_{-\infty}^{+\infty}\int(\left|\tilde{A}_{2+}\right|^2\left|F_{2+}\right|^4 + \left|\tilde{A}_{2-}\right|^2\left|F_{2-}\right|^2 F_{2+}F_{2+}^*)dxdy \tag{3.16c}$$

$$\Delta\tilde{\beta}_{2-} = \frac{k_0^2 n_{0-} n_2}{\beta_{2-}}\int_{-\infty}^{+\infty}\int(\left|\tilde{A}_{2-}\right|^2\left|F_{2-}\right|^4 + \left|\tilde{A}_{2+}\right|^2\left|F_{2+}\right|^2 F_{2-}F_{2-}^*)dxdy \tag{3.16d}$$

$$\kappa_{1+2+} = \frac{\omega^2\mu_1}{2\beta_{1+}}\int_{-\infty}^{+\infty}\int(\varepsilon_1 - \varepsilon_0)F_{1+}^* F_{2+}dxdy \tag{3.17a}$$

$$\kappa_{1-2+} = \frac{\omega^2 \mu}{2\beta_{1-}} \int\int_{-\infty}^{+\infty} (\varepsilon_1 - \varepsilon_0) F_{1-}^* F_{2+} dxdy \tag{3.17b}$$

$$\kappa_{1+2-} = \frac{\omega^2 \mu_1}{2\beta_{1+}} \int\int_{-\infty}^{+\infty} (\varepsilon_1 - \varepsilon_0) F_{1+}^* F_{2-} dxdy \tag{3.17c}$$

$$\kappa_{1-2-} = \frac{\omega^2 \mu_1}{2\beta_{1-}} \int\int_{-\infty}^{+\infty} (\varepsilon_1 - \varepsilon_0) F_{1-}^* F_{2-} dxdy \tag{3.17d}$$

$$\kappa_{2+1+} = \frac{\omega^2 \mu_1}{2\beta_{2+}} \int\int_{-\infty}^{+\infty} (\varepsilon_1 - \varepsilon_0) F_{2+}^* F_{1+} dxdy \tag{3.17e}$$

$$\kappa_{2-1+} = \frac{\omega^2 \mu_1}{2\beta_{2-}} \int\int_{-\infty}^{+\infty} (\varepsilon_1 - \varepsilon_0) F_{2-}^* F_{1+} dxdy \tag{3.17f}$$

$$\kappa_{2+1+} = \frac{\omega^2 \mu_1}{2\beta_{2+}} \int\int_{-\infty}^{+\infty} (\varepsilon_1 - \varepsilon_0) F_{2+}^* F_{1-} dxdy \tag{3.17g}$$

$$\kappa_{2-1+} = \frac{\omega^2 \mu_1}{2\beta_{2-}} \int\int_{-\infty}^{+\infty} (\varepsilon_1 - \varepsilon_0) F_{2-}^* F_{1-} dxdy \tag{3.17h}$$

In the neighborhood of the optical carrier frequency, ω_0 the $\bar{\beta}_{1,2\pm}$ can be calculated using Taylor series expansion

$$\bar{\beta}_{1,2\pm} = \beta_{1,2\pm} + (\omega - \omega_0)\beta_{1,2\pm}^{'} + \frac{1}{2}(\omega - \omega_0)^2 \beta_{1,2\pm}^{''} + \frac{1}{6}(\omega - \omega_0)^3 \beta_{1,2\pm}^{'''} + \ldots \tag{3.18}$$

where $\beta_{1,2\pm}^{'}$ links group velocity ($v_{g1,2\pm}$) while $\beta_{1,2\pm}^{''}$ and $\beta_{1,2\pm}^{'''}$ stand for group velocity dispersion (GVD) and third order dispersion (TOD) parameters, respectively. The TOD and higher-order terms in this expansion are generally negligible if the spectral width $\Delta\omega \ll \omega_0$, then we have

$$\bar{\beta}_{1,2\pm} = \beta_{1,2\pm} + (\omega - \omega_0)\beta_{1,2\pm}^{'} + \frac{1}{2}(\omega - \omega_0)^2 \beta_{1,2\pm}^{''} \tag{3.19}$$

One should convert equations from frequency domain to time domain by integrating the frequency components using Fourier transformation technique. In the transformation, in the time domain the operator $j\partial/\partial t$, $-\partial^2/\partial t^2$ correspond to simply multiplication by $\omega - \omega_0$, $(\omega - \omega_0)^2$, respectively. After some mathematical procedures, we can obtain the coupled nonlinear equations for the evolution of pulses with LCP and RCP components in the coupling region

$$\frac{\partial A_{1+}}{\partial z}+\delta_{1+}^{'}\frac{\partial A_{1+}}{\partial t}+j\beta_{1+}^{''}\frac{1}{2}\frac{\partial^2 A_{1+}}{\partial t^2}+j\wp A_{1+}=j\kappa_{1+2+}A_{2+}+j\kappa_{1+2-}A_{2-}+j\left(\gamma_{1+}\left|A_{1+}\right|^2+C_{1+}\left|A_{1-}\right|^2\right)A_{1+} \tag{3.20a}$$

$$\frac{\partial A_{1-}}{\partial z}+\delta_{1-}^{'}\frac{\partial A_{1-}}{\partial t}+j\beta_{1-}^{''}\frac{1}{2}\frac{\partial^2 A_{1-}}{\partial t^2}+j\wp A_{1-}=j\kappa_{1-2-}A_{2-}+j\kappa_{1-2+}A_{2+}+j\left(\gamma_{1-}\left|A_{1-}\right|^2+C_{1-}\left|A_{1+}\right|^2\right)A_{1-} \tag{3.20b}$$

$$\frac{\partial A_{2+}}{\partial z}+\delta_{2+}^{'}\frac{\partial A_{2+}}{\partial t}-j\beta_{2+}^{''}\frac{1}{2}\frac{\partial^2 A_{2+}}{\partial t^2}+j\wp A_{2+}=j\kappa_{2+1+}A_{1+}+j\kappa_{2+1-}A_{1-}+j\left(\gamma_{2+}\left|A_{2+}\right|^2+C_{2+}\left|A_{2-}\right|^2\right)A_{2+} \tag{3.20c}$$

$$\frac{\partial A_{2-}}{\partial z}+\delta_{2-}^{'}\frac{\partial A_{2-}}{\partial t}-j\beta_{2-}^{''}\frac{1}{2}\frac{\partial^2 A_{2-}}{\partial t^2}+j\wp A_{2-}=j\kappa_{2-1-}A_{1-}+j\kappa_{2-1+}A_{1+}+j\left(\gamma_{2-}\left|A_{2-}\right|^2+C_{2-}\left|A_{2+}\right|^2\right)A_{2-} \tag{3.20d}$$

where $\delta_{1\pm}^{'}=\beta_{1+}^{'}\pm\mu\xi$ and $\delta_{2\pm}^{'}=\beta_{2+}^{'}\pm\mu\xi$. In the equations above, $\wp=\omega_0\mu\xi_c$ associated with chirality, $\gamma_{1,2\pm}$ and $C_{1,2\pm}$ describe the coefficient of self-phase modulation (SPM) and cross phase modulation (XPM) in both cores for LCP and RCP components, respectively, which can be defined as the mode overlapping integration with

$$\gamma_{1\pm}=\frac{k_0^2 n_{0\pm}n_2}{\beta_{1\pm}}\int_{-\infty}^{+\infty}\left|F_{1\pm}\right|^4 dxdy \tag{3.21a}$$

$$\gamma_{2\pm}=\frac{k_0^2 n_{0\pm}n_2}{\beta_{2\pm}}\int_{-\infty}^{+\infty}\left|F_{2\pm}\right|^4 dxdy \tag{3.21b}$$

and

$$C_{1\pm}=\frac{k_0^2 n_{0\pm}n_2}{\beta_{1\pm}}\int_{-\infty}^{+\infty}\left|F_{1\mp}\right|^2 F_{1\pm}F_{1\pm}^{*}dxdy \tag{3.22a}$$

$$C_{2\pm}=\frac{k_0^2 n_{0\pm}n_2}{\beta_{2\pm}}\int_{-\infty}^{+\infty}\left|F_{2\mp}\right|^2 F_{2\pm}F_{2\pm}^{*}dxdy \tag{3.22b}$$

The first and second terms on the right side of Eq. (3.20) represent the coupling of the component in a fixed waveguide with that in the opposite waveguide while the third and fourth terms which are in the bracket indicate the effect of SPM and XPM in the same waveguide, respectively. In fact, even the coupling is very weak, one can easily observe its accumulated

effects in long sections of chiral fibers. Equations (3.20) include both the linear and nonlinear coupling mechanisms between the optical components in the chiral fiber couplers.

3.3 Calculation of coupling coefficients

We begin by considering a lossless nonlinear chiral fiber couplers with identical fiber cores of radius a, separated by a distance d between their centers as shown in Figure 1.1. Here for calculating the coupling coefficients that have been presented Eq. (3.17), we assumed that $\beta_{1+} = \beta_{2+} = \beta_{+}$ and $\beta_{1-} = \beta_{2-} = \beta_{-}$ for chiral fiber coupler with symmetrical structures of the same size and shape.

According to the calculation formula of the coupling coefficient in the previous section (see Eq. (3.17)), the coupling coefficient depends on the transverse distribution of the mode field ($F_{1,2\pm}(x,y)$) and it is independent of z. The coupling coefficient can be obtained by substituting the Eigen mode field of the chiral fiber into the coupling coefficient formula obtained Eq. (3.17).

In order to simplify our discussion, we can reasonably use a Gaussian function to describe the mode field of the LCP and RCP components distribution as

$$F_{1\pm} = A_{1\pm} \exp\left(\frac{-x^2 - y^2}{W_{1\pm}^2}\right) \tag{3.23}$$

$$F_{2\pm} = A_{2\pm} \exp\left(\frac{-x^2 - y^2}{W_{2\pm}^2}\right) \tag{3.24}$$

where $F_{1,2\pm}$, $W_{1,2\pm}$ and $A_{1,2\pm}$, respectively, represent the field distribution, the waist radius and the amplitudes of the RCP and LCP light normalized by

$$\int_{-\infty}^{+\infty}\int \left|F_{i\pm}\right|^2 dxdy = 1 \qquad (i = 1,2) \tag{3.25}$$

so that we can obtain

$$A_{1\pm} = \sqrt{\frac{1}{\int_0^a \int_{-\sqrt{a^2-x^2}}^{\sqrt{a^2-x^2}} e^{\frac{-2x^2-2y^2}{W_{1\pm}^2}} dxdy}} \tag{3.26a}$$

$$A_{2\pm} = \sqrt{\frac{1}{\int_0^a \int_{-\sqrt{a^2-x^2}}^{\sqrt{a^2-x^2}} e^{\frac{-2x^2-2y^2}{W_{2\pm}^2}} dxdy}} \tag{3.26b}$$

We calculate the coupling coefficient namely, κ_{1+2+}, κ_{1+2-}, κ_{1-2-}, κ_{1-2+}, κ_{2+1+}, κ_{2+1-}, κ_{2-1-} and κ_{2-1+} by

$$\kappa_{1+2+} = \frac{\omega^2 \mu_1}{2\beta_+} \int\int_{-\infty}^{+\infty} (\varepsilon_1 - \varepsilon_0) F_{1+}^*(x,y) F_{2+}(x,y) dxdy$$
$$= \frac{\omega^2 \mu_1 A_{1+} A_{2+}}{2\beta_+} \int_0^a \int_{-\sqrt{a^2-x^2}}^{\sqrt{a^2-x^2}} (\varepsilon_1 - \varepsilon_0) \exp\left(\frac{-x^2-y^2}{W_{1+}^2}\right) \exp\left[\frac{-(x-d)^2-y^2}{W_{2+}^2}\right] dxdy \quad (3.27)$$

$$\kappa_{1+2-} = \frac{\omega^2 \mu_1}{2\beta_+} \int\int_{-\infty}^{+\infty} (\varepsilon_1 - \varepsilon_0) F_{1+}^*(x,y) F_{2-}(x,y) dxdy$$
$$= \frac{\omega^2 \mu_1 A_{1+} A_{2-}}{2\beta_+} \int_0^a \int_{-\sqrt{a^2-x^2}}^{\sqrt{a^2-x^2}} (\varepsilon_1 - \varepsilon_0) \exp\left(\frac{-x^2-y^2}{W_{1+}^2}\right) \exp\left[\frac{-(x-d)^2-y^2}{W_{2-}^2}\right] dxdy \quad (3.28)$$

$$\kappa_{1-2-} = \frac{\omega^2 \mu_1}{2\beta_-} \int\int_{-\infty}^{+\infty} (\varepsilon_1 - \varepsilon_0) F_{1-}^*(x,y) F_{2-}(x,y) dxdy$$
$$= \frac{\omega^2 \mu_1 A_{1-} A_{2-}}{2\beta_-} \int_0^a \int_{-\sqrt{a^2-x^2}}^{\sqrt{a^2-x^2}} (\varepsilon_1 - \varepsilon_0) \exp\left(\frac{-x^2-y^2}{W_{1-}^2}\right) \exp\left[\frac{-(x-d)^2-y^2}{W_{2-}^2}\right] dxdy \quad (3.29)$$

$$\kappa_{1-2+} = \frac{\omega^2 \mu_1}{2\beta_-} \int\int_{-\infty}^{+\infty} (\varepsilon_1 - \varepsilon_0) F_{1-}^*(x,y) F_{2+}(x,y) dxdy$$
$$= \frac{\omega^2 \mu_1 A_{1-} A_{2+}}{2\beta_-} \int_0^a \int_{-\sqrt{a^2-x^2}}^{\sqrt{a^2-x^2}} (\varepsilon_1 - \varepsilon_0) \exp\left(\frac{-x^2-y^2}{W_{1-}^2}\right) \exp\left[\frac{-(x-d)^2-y^2}{W_{2+}^2}\right] dxdy \quad (3.30)$$

$$\kappa_{2+1+} = \frac{\omega^2 \mu_1}{2\beta_+} \int\int_{-\infty}^{+\infty} (\varepsilon_1 - \varepsilon_0) F_{2+}^*(x,y) F_{1+}(x,y) dxdy$$
$$= \frac{\omega^2 \mu_1 A_{2+} A_{1+}}{2\beta_+} \int_0^a \int_{-\sqrt{a^2-x^2}}^{\sqrt{a^2-x^2}} (\varepsilon_1 - \varepsilon_0) \exp\left(\frac{-x^2-y^2}{W_{2+}^2}\right) \exp\left[\frac{-(x-d)^2-y^2}{W_{1+}^2}\right] dxdy \quad (3.31)$$

$$\kappa_{2-1-} = \frac{\omega^2 \mu_1}{2\beta_+} \int\int_{-\infty}^{+\infty} (\varepsilon_1 - \varepsilon_0) F_{2-}^*(x,y) F_{1-}(x,y) dxdy$$
$$= \frac{\omega^2 \mu_1 A_{2-} A_{1-}}{2\beta_-} \int_0^a \int_{-\sqrt{a^2-x^2}}^{\sqrt{a^2-x^2}} (\varepsilon_1 - \varepsilon_0) \exp\left(\frac{-x^2-y^2}{W_{2-}^2}\right) \exp\left[\frac{-(x-d)^2-y^2}{W_{1-}^2}\right] dxdy \quad (3.32)$$

$$\kappa_{2-1+} = \frac{\omega^2 \mu_1}{2\beta_+} \int_{-\infty}^{+\infty} \int (\varepsilon_1 - \varepsilon_0) F_{2-}^*(x,y) F_{1+}(x,y) dxdy$$
$$= \frac{\omega^2 \mu_1 A_{2-} A_{1+}}{2\beta_-} \int_0^a \int_{-\sqrt{a^2-x^2}}^{\sqrt{a^2-x^2}} (\varepsilon_1 - \varepsilon_0) \exp\left(\frac{-x^2-y^2}{W_{2-}^2}\right) \exp\left[\frac{-(x-d)^2-y^2}{W_{1+}^2}\right] dxdy \quad (3.33)$$

$$\kappa_{2+1-} = \frac{\omega^2 \mu_1}{2\beta_+} \int_{-\infty}^{+\infty} \int (\varepsilon_1 - \varepsilon_0) F_{2+}^*(x,y) F_{1-}(x,y) dxdy$$
$$= \frac{\omega^2 \mu_1 A_{2+} A_{1-}}{2\beta_+} \int_0^a \int_{-\sqrt{a^2-x^2}}^{\sqrt{a^2-x^2}} (\varepsilon_1 - \varepsilon_0) \exp\left(\frac{-x^2-y^2}{W_{2+}^2}\right) \exp\left[\frac{-(x-d)^2-y^2}{W_{1-}^2}\right] dxdy \quad (3.34)$$

It is very difficult for the above formula to get the result of the analysis. In fact, one can use the numerical method to calculate the coupling coefficients. From the above expression, it can be seen that the magnitude of the coupling coefficient depends on the propagation constant, the radius of the fiber, and the distance between the fibers. Here we choose the radius $a = 2\,\mu\text{m}$, the distance between the two fiber cores $d = 50\,\mu\text{m}$, chiral parameter $\xi = 2\times10^{-4}$ mho, dielectric constant $\varepsilon_1 = 2\times10^{-12}$ F/m and magnetic permeability μ_0. The calculated coupling coefficients are as follows $\kappa_{1+2+} = 1308.3\,\text{m}^{-1}$, $\kappa_{1-2-} = 1312.9\,\text{m}^{-1}$, $\kappa_{1-2+} = 188.2\,\text{m}^{-1}$, $\kappa_{1+2-} = 912.7\,\text{m}^{-1}$, $\kappa_{2+1+} = 1312.9\,\text{m}^{-1}$, $\kappa_{2-1-} = 1316.9\,\text{m}^{-1}$, $\kappa_{2-1+} = 1887.7\,\text{m}^{-1}$ and $\kappa_{2+1-} = 915.4\,\text{m}^{-1}$. Therefore, when the radius of the fiber and the distance between the cores are both fixed, each chiral parameter is assigned a value of a set of coupling coefficients.

Equations (3.20) can be converted to the set of normalized GCCNLSEs which can be written as

$$j\frac{\partial U_{1+}}{\partial Z} + \frac{1}{2}\frac{\partial^2 U_{1+}}{\partial \tau^2} + \wp U_{1+} + \gamma\left(|U_{1+}|^2 + \delta|U_{1-}|^2\right)U_{1+} + \kappa_{1+2+}U_{2+} + \kappa_{1+2-}U_{2-} = 0 \quad (3.35a)$$

$$j\frac{\partial U_{1-}}{\partial Z} + \frac{1}{2}\frac{\partial^2 U_{1-}}{\partial \tau^2} + \wp U_{1-} + \gamma\left(|U_{1-}|^2 + \delta|U_{1+}|^2\right)U_{1-} + \kappa_{1-2-}U_{2-} + \kappa_{1-2+}U_{2+} = 0 \quad (3.35b)$$

$$j\frac{\partial U_{2+}}{\partial Z} + \frac{1}{2}\frac{\partial^2 U_{2+}}{\partial \tau^2} + \wp U_{2+} + \gamma\left(|U_{2+}|^2 + \delta|U_{2-}|^2\right)U_{2+} + \kappa_{2+1+}U_{1+} + \kappa_{2+1-}U_{1-} = 0 \quad (3.35c)$$

$$j\frac{\partial U_{2-}}{\partial Z} + \frac{1}{2}\frac{\partial^2 U_{2-}}{\partial \tau^2} + \wp U_{2-} + \gamma\left(|U_{2-}|^2 + \delta|U_{2+}|^2\right)U_{2-} + \kappa_{2-1-}U_{1-} + \kappa_{2-1+}U_{1+} = 0 \quad (3.35d)$$

where $\gamma = \gamma_{i\pm}$ $(i = 1,2)$ and $\delta = C/\gamma$ with $C = C_{i\pm}$ $(i = 1,2)$. In the above equations $U_{1\pm} = (\gamma L_D)^{1/2} A_{1\pm}$ and $U_{2\pm} = (\gamma L_D)^{1/2} A_{2\pm}$ represent the normalized amplitudes while $Z = z/L_D$ and $\tau = T_0/T$ indicate the

normalized distance and normalized time in which L_D and T_0 corresponds the dispersion length and the pulse width.

3.4 Numerical Method

In order to reveal the new effects that the chirality and coupling bring into the interaction of LCP and RCP ones in the evolution of pulses, we simulate pulse propagation based on Eq. (3.35) for different parameters. For this purpose, we consider an unchirped Gaussian input pulse. For simplicity and without loss of generality, linear and nonlinear effects are treated separately.

There are several numerical methods that can be applied, for instance, the split-step Fourier (SSF) method [105], finite-difference-time-domain (FDTD) method [106, 107] and double-grid finite-difference frequency-domain (DG-FDFD) method. Among these methods, the SSF method has the advantage of simplicity. Moreover, for the special case of nonlinear fiber optics, the most used numerical algorithms is the SSF method [4]. This algorithm simulates the propagation of light in optical fiber step by step considering either dispersion or nonlinearity at a time [108]. In other words, the fiber is treated as a dispersive (linear) in the frequency domain; and nonlinear in the time domain. The reason lies in the fact that the NLSE's solution is known for pure nonlinearity in the time domain and for pure dispersion in the frequency domain.

3.4.1 Split-step Fourier method

The split-step Fourier (SSF) method is a pseudo-spectral numerical method used to solve nonlinear partial differential equations such as NLSE [4, 109]. The name arises for two reasons. First, the method relies on computing the solution in small steps, and treating the linear and the nonlinear steps separately. Second, it is necessary to Fourier transform back and forth because the linear step is made in the frequency domain while the nonlinear step is made in the time domain [4, 109]. This method is used in the field of light pulse propagation in optical fibers, where the interaction of linear and nonlinear mechanisms makes it difficult to find general analytical solutions. However, the split-step method provides a numerical solution to the problem. Use of fast Fourier transform (FFT) improves the speed of the computation [4, 109]. In general the classical nonlinear Schrodinger equation (NLSE) describes the dispersion and nonlinearity which act together in optical waveguide [3, 110].

The main idea of SSFM is to find approximate solutions of NLSE by assuming that the diffraction and nonlinear effects act independently [109, 111]. Here we split the propagation of the field in two steps:

one for diffraction only and one for nonlinear propagation only. Moreover, we calculate the linearly propagating field by working in the Fourier space [109, 111].

3.4.2 Finite element method

Finite element method (FEM) is a numerical method that proposes an approximate solution to the boundary value problem [113, 114]. Starting from 1940's the FEM has a history of solving boundary value problem in mathematics and physics [114, 115]. This method was initially focused on aircraft design. Later it was adopted by the civil engineers for structural design [114, 115]. Today the method is extended for many other areas of physics and engineering. An approximate solution to any complex engineering problem can be reached by subdividing the problem into smaller more manageable (finite) elements [114, 115]. Using finite elements, solving complex partial differential equations that describe the behavior of certain structures can be reduced to a set of linear equations that can be easily solved using the standard techniques of matrix algebra [113, 114].

FEM is a unique numerical method which addresses problems in areas of physics and engineering that include fluid mechanics, mechanics of materials, chemical reactions, semiconductor devices, electromagnetics, optics, quantum mechanics, acoustics etc. The key features of FEM are [114, 115]

(1) Piecewise approximation of continuous field gives good precision even with the simple approximating functions.

(2) Using computational time and resources we can improve the precision just by increasing the number of elements.

(3) FEM analysis approximates the element of small sizes and different shapes. This eases the application of complex shape of different materials and different boundary conditions.

(4) It covers both linear and nonlinear problems.

(5) Local approximation generates a sparse system of equation that helps to solve the problem having a large number of model unknown.

The finite element method was applied to the analysis of photonic crystal fibers in 2000 and has since been used extensively to analyze other types of fiber structures [116]. For the photonic crystal fiber, we must first consider the mode field distribution, in order to obtain accurate cross-sectional field distribution of optical fiber, you need to choose a set of basic subspace (element) to solve Maxwell differential equation. It is necessary to consider the continuity condition of the field, which divides the cross section of the fiber into distinguishable isotropic subspaces. This distinction leads to a simple finite

element mesh: a triangle or a quadrilateral. The FEM allows discretization of different sizes, which depends mainly on the waveguide structure and the expected mode response. The proper description of the field makes the distance from the discrete subspace to the center core shorter, which makes the size of the selection computation smaller. Discrete Maxwell equations for each element, resulting in a set of elementary element matrices. The arrangement of these base matrices creates an integral matrix system of the complete structure under study. According to this matrix, the distribution of polarization modes and the effective refractive index can be calculated. In this case, continuity conditions must be considered for each subspace boundary.

Finite element method has been applied to the study of the structure of the traditional optical fiber waveguide, there are no reports of the chiral fiber waveguide. For complex waveguides, the discrete-time structure is complex and computationally intensive due to a large number of variables and small size. Therefore, this method is not used in this dissertation.

3.4.3 Finite difference time domain method

Finite-difference time-domain method (FDTD) was proposed by Qiu in 2001 to study the guided modes of photonic crystal fibers [117]. FDTD method has been successfully applied to calculate the in-plane and out-of-plane energy band structures of photonic crystals and to calculate the defect modes, waveguide modes, and surface modes. Based on the variational principle and the interpolation method, the solution region is divided into several small regions. The field functions of each region are represented by trial solutions with unknown coefficients. Then the differential equation is used to transform the differential equation into coefficient of the algebraic equation, combined with boundary conditions to solve. It should be noted that the FDTD method is not based on a modal method, and the transmission field in a multimode waveguide structure can be regarded as the summation of the excitation modes. The finite-difference-time-domain method is flexible, in different conditions, the need for appropriate design boundary conditions. In addition, the discrete space and time step will affect the calculation time and accuracy. The smaller the step size is, the higher the accuracy is, but the calculation time and the computer memory requirement are increased. At this time, the time and space steps need to be designed with the precision.

As the electromagnetic wave propagation in chiral media, there is magnetic coupling, has been the development of chiral FDTD method is used in the double-grid method, that is, conventional Yee grid superimposed on the basis of the second layer Yee grid. All the field components to find their appropriate

location, while the conventional finite difference time-domain method to ensure the stability of this difference format can be. At present, the chiral FDTD method has not been applied to the study of photonic crystal structures. Compared with the plane wave expansion method, this method is not suitable for the boundary condition setting, space discrete simulation is difficult, and the calculation is large, so this method is not used in this paper.

3.4.4 Double grid finite difference frequency domain method

The finite difference method in the frequency domain can be used directly from the Maxwell equations. The Yee grids are used to discretized space, and the partial differentials in the equations are approximated to the central difference on the grid nodes, and a set of difference equations is obtained. After solving, we get the corresponding field value of each node. Because the electric field nodes and the magnetic field nodes in the Yee grid are interdigitated, and the uniform Yee grid is used to discretized space, the resulting difference equation has the second-order algebraic precision.

Compared with the FDTD method, the FD-FDTD method can obtain the parameters such as propagation constant, mode field distribution and loss. The finite-difference method can be applied to almost all kinds of fiber structures. The computational cost of this method is related to the cross-section size and dispersion precision of the fiber. When the cross-section is large and the precision of the dispersion is high, the computational cost is greatly increased, but the calculation accuracy is high. In order to balance this contradiction, the boundary conditions can be appropriately set in consideration of the symmetry of the mode field, and the same result can be obtained by calculating only a part of the cross-section of the optical fiber.

The chiral FDTD method has been developed to study the Maxwell nonlinear Schrödinger System [118]. This approach is stable in the long wavelength regime and removes the need to extract the potentials at every time step. The perfectly matched layer (PML) important for FDTD simulations is developed for this new approach.

Among these mentioned methods, the SSF method has the advantage of simplicity. Moreover, for the special case of nonlinear fiber optics, the most used numerical algorithms is the SSF method [4]. This algorithm simulates the propagation of light in optical fiber step by step considering either dispersion or nonlinearity at a time [108]. In other words, the fiber is treated as a dispersive (linear) in the frequency domain; and nonlinear in the time domain. The reason lies in the fact that the NLSE's solution is known for pure nonlinearity in the time domain and for pure dispersion in the frequency domain.

3.4.5 Low power conditions

Firstly, we consider the linear case i.e. when the continuous wave (CW) with low power is incident into the fiber, the change of the refractive index in the fiber can be ignored reasonably. Thus, we set the nonlinear terms to be zero ($\gamma = 0$) in the Eq. (3.35). Then, Eq. (3.35) can be rewritten in terms of matrix and vector as

$$\frac{d}{dz}\mathbf{U}(z) = \mathrm{M}\,\mathbf{U}(z) \tag{3.36}$$

here $U(z) = \left(U_{1+}(z)U_{1-}(z)U_{2+}(z)U_{2-}(z)\right)^T$. $U_{1\pm}(z)$ and $U_{2\pm}(z)$ represent the magnitudes of the LCP and RCP components in the optical fibers 1 and 2, respectively, and M stands for a matrix composed of the coupling coefficient and the propagation constant which can be written as

$$\mathrm{M} = j\begin{pmatrix} \wp & 0 & \kappa_{2+1+} & \kappa_{2-1+} \\ 0 & \wp & \kappa_{2+1-} & \kappa_{2-1-} \\ \kappa_{1+2+} & \kappa_{1-2+} & \wp & 0 \\ \kappa_{1+2-} & \kappa_{1-2-} & 0 & \wp \end{pmatrix} \tag{3.37}$$

one can defined the coupling length of the chiral coupler as L. The initial condition is accepted for the single component single port incidence, namely $U_{1+}(0) = U_{0+}$.

3.4.6 Runge-Kutta method

Runge-Kutta method (RKM) is one of the most commonly used numerical methods to solve an initial value problem (IVP) described by a system of ordinary differential equations (ODEs). RKM is the ideal method for solving system of ODEs with smoothly varying coefficients.

At the first application of RKM to advance the vector functions $\mathbf{U}(0)$ in Eq. (3.36) to the next step $\mathbf{U}(dz)$, we find that part of the initial conditions are missing. To make RKM work, we must update $\mathbf{U}(\mathbf{z})$ vectors due to all possible initial conditions. In other words, we need to compute the transfer-function matrix that will take us from any arbitrary initial vector $\mathbf{U}(\mathbf{z})$ to $\mathbf{U}(dz)$ and eventually to $\mathbf{U}(L)$. We begin RKM process by first dividing the grating region $0 < z < L$ into m equally spaced sections, each with a length $h = L/m$. The centered position of the ith section is $z_i = (i - 1/2)h$ for $i = 1,...m$. When we apply the fourth-order RKM method, the local transfer-function $\mathbf{R}_i$ is written as

$$\mathbf{R}_i = \mathbf{I} + (2\mathbf{k}_{1i} + 2\mathbf{k}_{2i} + \mathbf{k}_{3i} + \mathbf{k}_{4i})/6 \tag{3.38}$$

where matrices $\mathbf{k}_{1i}, \mathbf{k}_{2i}, \mathbf{k}_{3i}$ and $\mathbf{k}_{4i}$ are intermediate Runge-Kutta calculations given by

$$\begin{aligned}
\mathbf{k}_{1i} &= h\mathbf{U}(z = ih - h) \\
\mathbf{k}_{2i} &= h\mathbf{U}(z = ih - h/2)(\mathbf{I}+\mathbf{k}_{1i}/2) \\
\mathbf{k}_{3i} &= h\mathbf{U}(z = ih - h/2)(\mathbf{I}+\mathbf{k}_{2i}/2) \\
\mathbf{k}_{4i} &= h\mathbf{U}(z = ih)(\mathbf{I}+\mathbf{k}_{3i}/2)
\end{aligned} \tag{3.39}$$

Each $\mathbf{R}_i$ connects the two amplitude vectors at the two ends of the section as

$$\mathbf{U}(ih) = \mathbf{R}_i \cdot \mathbf{U}\left[(i-1)h\right] \tag{3.40}$$

These transfer-function matrices $\mathbf{R}_i$ i = 1, ..., m, help to connect the amplitude vector $\mathbf{U}$ at $z = L$ with $\mathbf{U}$ at z = 0 in the following way:

$$\begin{aligned}
\mathbf{U}(L) = \mathbf{U}(mh) &= \mathbf{R}_m \cdot \mathbf{U}\left[(m-1)h\right] \\
&= \mathbf{R}_m \cdot \mathbf{R}_{m-1} \ldots \mathbf{R}_1 \cdot \mathbf{U}(0) = \mathrm{G}_{RKM1} \cdot \mathbf{U}(0)
\end{aligned} \tag{3.41}$$

Matrix G_{RKM1} is the global transfer matrix computed by Runge-Kutta method for solving z-dependent coefficient Eq. (3.36). The transmission and refection efficiencies of the core mode can be expressed as

$$T_{1\pm} = \frac{\left|U_{01\pm}(L)\right|^2}{\left|U_{001\pm}(0)\right|^2} = \left|U_{01\pm}(L)\right|^2 \tag{3.42}$$

$$T_{2\pm} = \frac{\left|U_{02\pm}(L)\right|^2}{\left|U_{002\pm}(0)\right|^2} = \left|U_{02\pm}(L)\right|^2 \tag{3.43}$$

where $U_{01\pm}$ and $U_{02\pm}$ are the first element of $U_{01\pm}(L)$ and $U_{02\pm}(L)$, respectively. To get the analytical solution for Eq. (3.36), here we employ numerical simulation based on Runge-Kutta method.

We simulate the coupled characteristic of the two chiral fibers using Eq. (3.36) and the following parameters: $\lambda = 1.55\,\mu\mathrm{m}$ (wavelength), $a = 2\lambda$ (core-radius), $d = 2a$ (distance between the two cores), $\mu_1 = 1.2692 \times 10^{-6}\,\mathrm{H}$ (the permeability of the core layer), $\xi_c = 1 \times 10^{-5}$ mho (chiral parameter), while $\varepsilon_1 = 1.3813 \times 10^{-11}\,\mathrm{F/m}$ (the dielectric constant of the core layer).

4. Result and Discussion

In order to reveal the new effects that the chirality and linear coupling bring into the interaction of LCP and RCP ones in the evolution of pulses, we simulate pulse propagation based on Eq. (16) for different parameters. For this purpose, we consider an unchirped Gaussian input pulse. To make our discussion simple, linear and nonlinear effects are treated independently. Firstly, we consider the case of linear effects i.e., when the incident light is continuous wave (CW) and low power, the refractive index of the coupler is not changed with the light power.

4.1 Low Energy Conditions

When the input beam is a low-energy beam, we can remove the nonlinear term in the nonlinear coupled mode equation of the chiral fiber, that is, the γ and δ (nonlinear distribution term) in Eq. (16) is set to be zero. Thus, according to the coupled-mode equation, Eq. (16) in term of the matrix can be written as

$$\frac{d}{d\zeta}\begin{pmatrix} U_{1+}(\zeta) \\ U_{1-}(\zeta) \\ U_{2+}(\zeta) \\ U_{2-}(\zeta) \end{pmatrix} = j\begin{pmatrix} \wp & 0 & \kappa & 0 \\ 0 & \wp & 0 & \kappa \\ \kappa & 0 & \wp & 0 \\ 0 & \kappa & 0 & \wp \end{pmatrix}\begin{pmatrix} U_{1+}(\zeta) \\ U_{1-}(\zeta) \\ U_{2+}(\zeta) \\ U_{2-}(\zeta) \end{pmatrix}. \tag{4.1}$$

By using the boundary condition that a single CW beam is launched into waveguide 1 such that $U_{1\pm}(0) = U_{0\pm}$ and $U_{2\pm}(0) = 0$, the solutions of Eq. (4.1) is given by

$$U_{1\pm}(\zeta) = \exp(j\beta\zeta)\left[U_{1\pm}(0)\cos(\kappa_{eff}\zeta) + jU_{2\pm}(0)(\wp/\kappa_{eff})\sin(\kappa_{eff}\zeta)\right], \tag{4.2a}$$

$$U_{2\pm}(\zeta) = \exp(j\beta\zeta)\left[jU_{1\pm}(0)(\wp/\kappa_{eff})\sin(\kappa_{eff}\zeta) + U_{2\pm}(0)\cos(\kappa_{eff}\zeta)\right], \tag{4.2b}$$

where the effective coupling coefficient κ_{eff} is defined as $\kappa_{eff} = \sqrt{\kappa^2 + \wp^2}$. From Eqs. (4.2) one can obtain the output powers by $P_{1\pm}(\zeta) = |U_{1\pm}(\zeta)|^2$ and $P_{2\pm}(\zeta) = |U_{2\pm}(\zeta)|^2$ which can be given by $P_{1\pm}(\zeta) = P_{0\pm}\cos^2(\kappa\zeta)$ and $P_{2\pm}(\zeta) = P_{0\pm}\sin^2(\kappa\zeta)$. The ratio of output to input power on $(\kappa/\kappa_{eff})\zeta$, in fact, κ_{eff} depends on the chiral parameter. The maximum power is transferred occurs $\kappa_{eff}\zeta = m\pi/2$, where m are an integer and the coupling length can be given by $\zeta_c = \pi/(2\kappa_{eff})$.

On plotting the figures, matrix transfer method and the following parameters are used: wavelength $\lambda = 1.55\,\mu m$, core-radius $a = 2\lambda$, core spacing between the cores $d = 2a$, chiral parameter $\xi_{\pm} = \pm 1\times10^{-5}\,mho$, the permeability constant of the core layer $\mu_1 = 1.2692\times10^{-6}\,H$, the

dielectric constant of the cladding $\mu_2 = \mu_0$, the dielectric of the core layer $\varepsilon_1 = 8.9427 \times 10^{-12}\, F/m$, the permeability of the cladding $\varepsilon_2 = \varepsilon_0$ and refractive index $n_2 = 2.35 \times 10^{-13}\, m^2/W$.

Note that in the following Figures, P_{1+} and P_{1-} indicates RCP and LCP in waveguide 1wheras. P_{2+} and P_{2-} represents RCP and LCP in waveguide 2. Figure 4.1 shows that initial power in fiber 1 decrease gradually and transferred to the waveguide 2. As seen from Figure 4.1 (a) the LCP and RCP light have two different coupling mechanisms when the light is transmitted in the chiral fiber couplers. In the same transmission distance, LCP and RCP light have different transmission periods. The transmission period of the LCP light is greater than that of RCP light and the power of the RCP light alternates faster than that of the LCP light. From this figure, we can see that the chiral fiber 1 contains only RCP (LCP=0) light and the chiral fiber 2 contains LCP (RCP=0) light at the coupling length of $0.5 \times 10^{-3}\, m$.

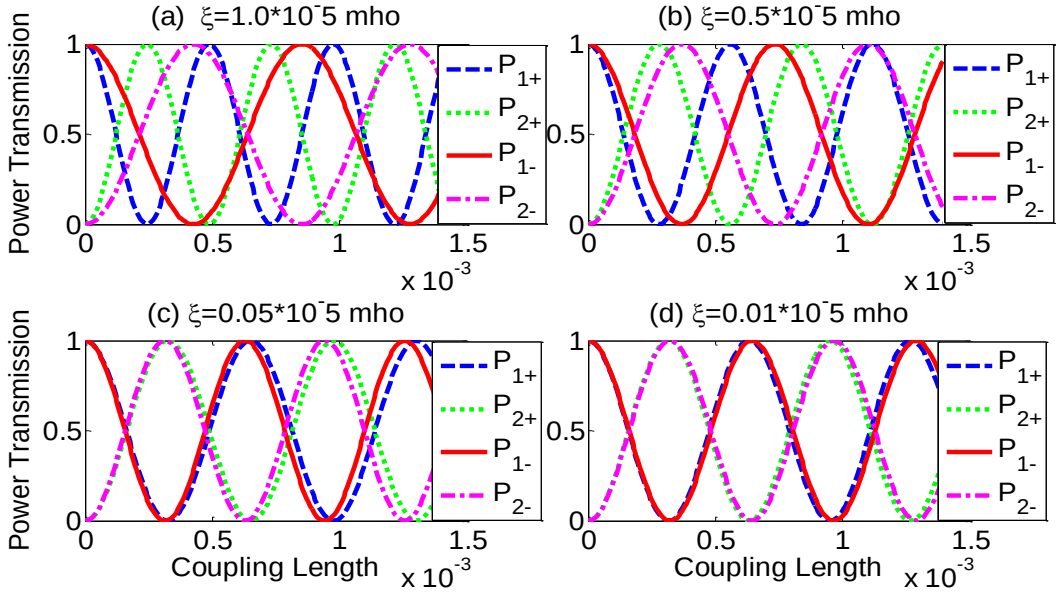

Figure 4.1 Periodic power transfer between and through cores with core spaced $d = 2.25a$

In this case, one can achieve the separation of power. Thus, the function of the polarizer can be realized. On the contrary, Figure 4.1 (b) illustrates that no separation of LCP and RCP light during their propagation when the core spacing change from $d = 2.25a$ to $d = 2.55a$. At the transmission distance $0.3\, mm$ and $1\, mm$ the output powers of two waveguides is equal i.e. 1:1 ratio can be achieved, in which 3 dB coupler can be implemented. At the coupling length of $0.6\, mm$ and $1.2\, mm$ the light power totally outputs from waveguide 2 and 1, respectively in which

0:1 and 1:0 ratios can be realized. Thus, the choice of output depends on the couplers length to achieve the optical switch. When the distance between two fiber couplers exceeds $d = 2.55a$, the LCP and RCP light in the chiral fibers are separated again and the power is redistributed (see Figure 4.1 (c)). From this figure, we find that the coupling of RCP and LCP light in both waveguides become very weak and the energy exchange is slower. It can be concluded that when the distance between the two optical fibers reaches a certain level, neither the LCP light nor the RCP light is coupled during their propagations.

In Figurer 4.1 we have discussed the coupling characteristics of LCP and RCP light by changing the separation distance between the two chiral fiber couplers and keeping the chiral parameter constant. In Figure 4.2 below the distance between the two fibers kept fixed at $d = 2.55a$ the coupling of RCP and LCP light in both cores under different chiral parameters are demonstrated. From Figure 4.2 one can realize that the separation of the LCP and RCP light becomes difficult with the decrease of the chiral strength.

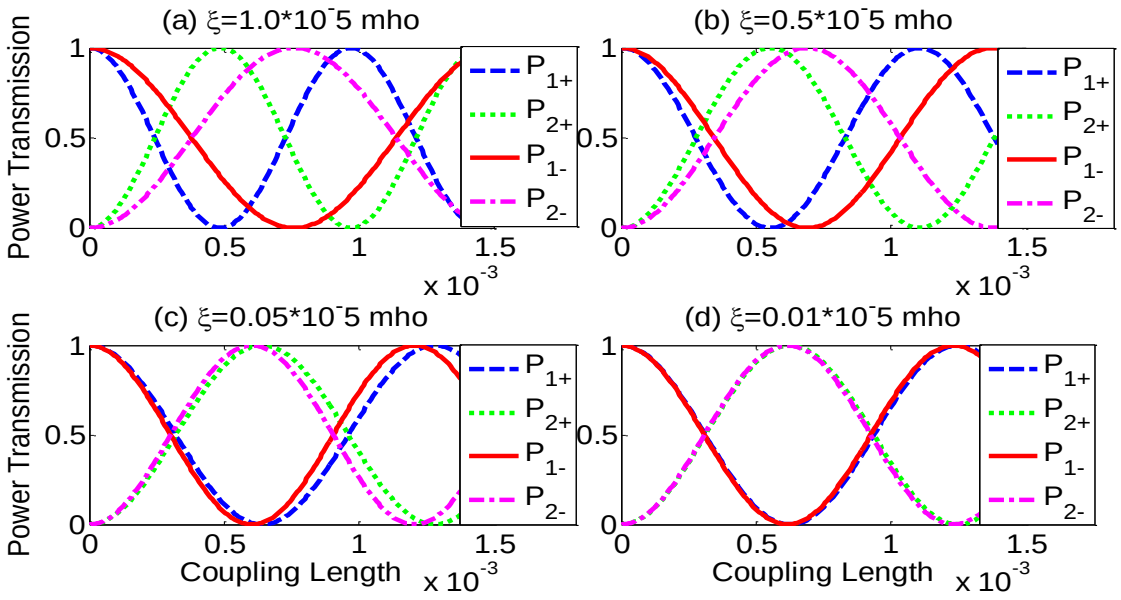

Figure 4.2 Periodic power transfer between and through cores with core spaced $d = 2.55a$

Comparing Figure 4.2 (a) and Figure 4.1 (a), the difference between the two figures is that the core spacing has changed from $d = 2.25a$ to $d = 2.55a$. When the core spacing is maintained at the aforementioned fixed value $d = 2.55a$, the chiral parameter is changed and the power transmission of each polarization component in the chiral fiber changes. Therefore, the

separation of LCP and RCP components of chiral fibers can be achieved by adjusting the chiral parameters.

From Figure 4.2 we found that with the reduction of the chiral parameters, the separation of LCP and RCP light is less and less obvious. When the chiral parameter decreases slowly to $\xi_{\pm} = \pm 0.05 \times 10^{-5}$ mho, the LCP and RCP components are no longer separated and the chiral optical fiber shows the same coupling property as the traditional fiber couplers (see Figure 4.1 (c) and Figure 4.2 (c)). As a result, the optical power distribution can still be achieved with both waveguides.

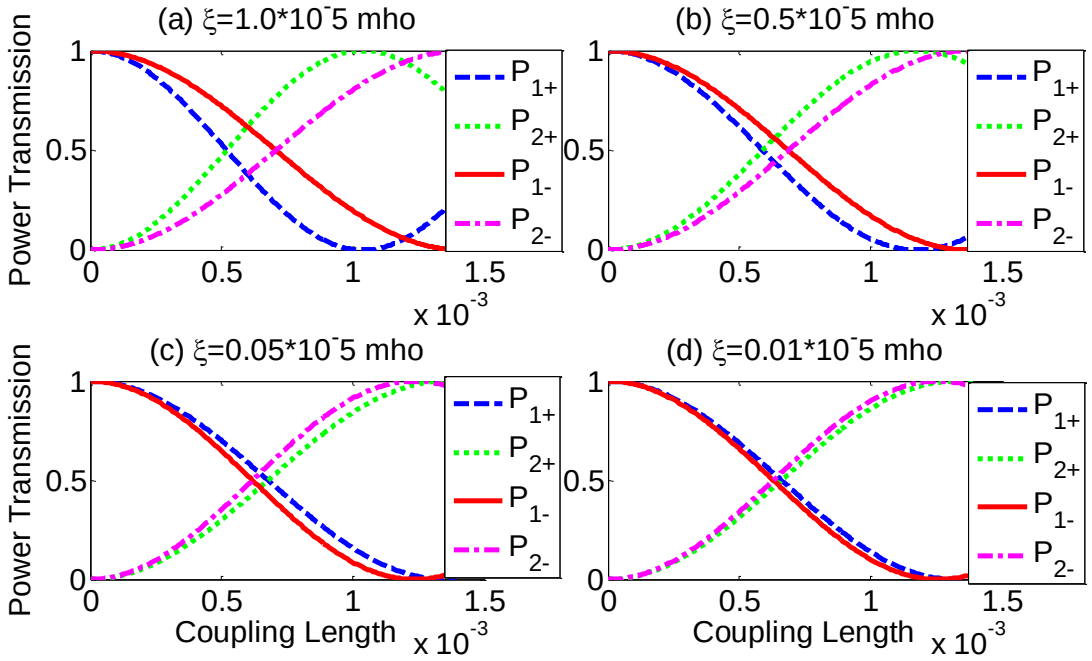

Figure 4.3 Periodic power transfer between and through cores at with core spaced $d = 2.55a$

Earlier we have discussed the variation of the transmission power of different polarization components in the two arms of the coupler with varying the coupling length. Now, we have launched single polarization (say right circular polarization) to one port of the coupler to study characteristics of the coupler. In fact, its output polarization change is very important for us to discuss the optical output characteristics of the coupler. Figure 4.4 shows the variation of the output polarization state of the coupler arms with the coupling length under different chiral parameters. The initial incident conditions at this time are the same as above.

Figure 4.4 shows the transmission dependences of power on the coupling length for the opposite components with different chiral parameters. From Figure 4.4 one can see that the

initial power (RCP component) in fiber 1 decreases gradually and transferred to the fiber 2 (RCP and LCP components) and LCP in fiber 1. When the chiral parameter is very small, inter coupling mechanism is much stronger than the mutual coupling one and the interaction between the LCP and RCP components in fiber 1 is also stronger than the interaction between LCP and RCP components in the fiber 2 as the initial power is introduced into fiber (see Figure 4.4 (a)). In fiber 2, the periodic of change of two polarization components is almost close except that the maximum value is slightly different, while in fiber 1, the RCP and LCP components alternate periodically. When chirality strength increases from $\xi_c = 3\times10^{-6}$ mho to $\xi_C = 8\times10^{-6}$ mho inter coupling mechanism tends to decrease gradually while the mutual coupling one increases as seen from Figure 4.4 (b), (c) and (d).

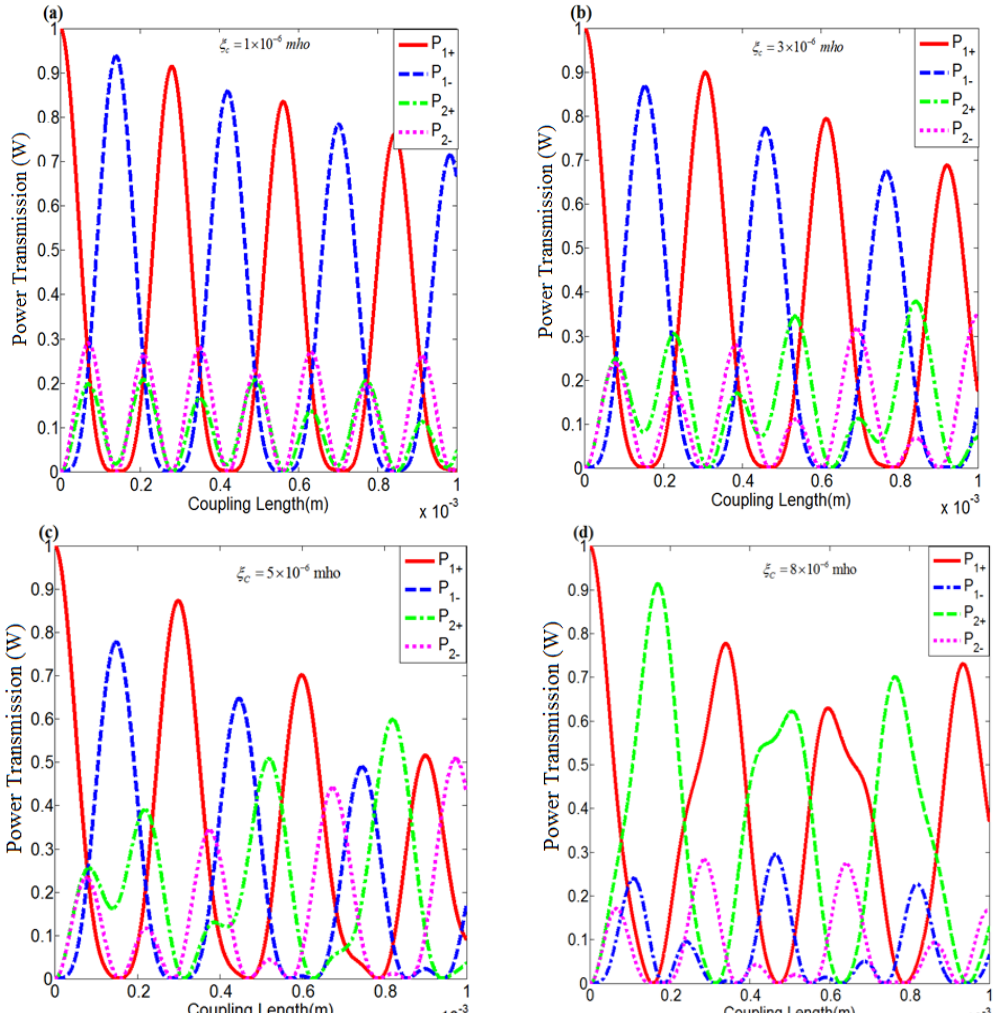

Figure 4.4 The transmission power of LCP and RCP component in two arms of coupler versus coupling length for weak chirality strength.

From these Figures one can see that the maximum power of the RCP and LCP components in fiber 1 decrease as the coupling length increases, with the reduced power being coupled into the fiber 2 components. The maximum power of two polarization components in fiber 2 increase, and they suppress each other.

As the chiral strength increase, the amplitude of LCP components in the two fibers continue to compress and dominated by the RCP components in both fibers. From Figure 4.5 (a), (b) and (c) one can see that the amplitude of LCP components in both fibers are ever more decrease as the chiral strength continues to increase from $\xi_c = 1\times10^{-5}$ mho to $\xi_C = 8\times10^{-5}$ mho and the power of the LCP component in the two fibers periodically overlap when $\xi_c = 5\times10^{-5}$ mho.

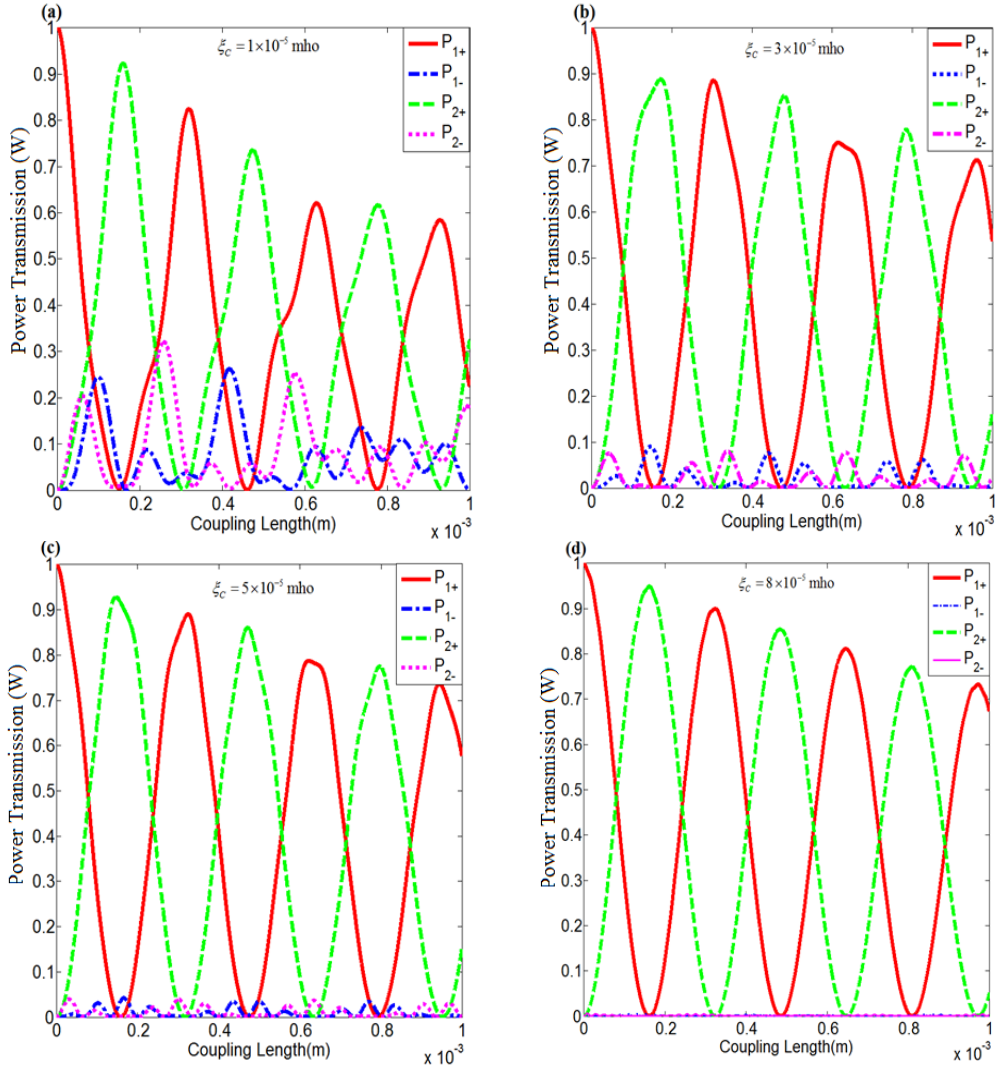

Figure 4.5 The transmission power of LCP and RCP component in two arms of coupler versus coupling length for strong chirality strength.

As can be seen from Figure 4.5 (d), when the chiral parameter become more stronger, namely $\xi_C = 8\times10^{-5}$ mho, only the RCP components exist in both fibers, and their transmission power alternates periodically. When the coupling length is 0.16 mm, 0.50 mm, 0.81 mm, the power in the optical fiber 1 completely coupled into the fiber 2 while when the coupling length is 0.33 mm, 0.82 mm, 0.97 mm, the power in the fiber 2 completely coupled into the optical fiber 1. When the coupling length is 0.083 mm, 0.24 mm, 0.42 mm, 0.58 mm, 0.72 mm, 0.88 mm the power in the two optical fibers is equal. Thus, we can take advantage of this nature of chiral couplers to make 3dB couplers for circularly polarized light by choosing the appropriate chirality parameter strength and coupling length.

4.2 Nonlinear Effects

Now, we consider the roles of nonlinearity separately by ignoring the dispersion of quasi-continuous beams propagating through nonlinear chiral fiber couplers. In this case, Eq. (16) can be rewritten as

$$\frac{dU_{1\pm}}{dz} = j\kappa_{1\pm2\pm}U_{2\pm} + j\gamma\left(|U_{1\pm}|^2 + \delta|U_{1\mp}|^2\right)U_{1\pm}, \tag{4.3a}$$

$$\frac{dU_{2\pm}}{dz} = j\kappa_{2\pm1\pm}U_{1\pm} + j\gamma\left(|U_{2\pm}|^2 + \delta|U_{2\mp}|^2\right)U_{2\pm}. \tag{4.3b}$$

The normalized component amplitudes can be expressed as

$$U_{i\pm} = \sqrt{P_{i\pm}}\exp(j\phi_{i\pm}) \quad (\mathrm{i}=1,2), \tag{4.4}$$

where $P_{i\pm}$, $\phi_{i\pm}$ $(\mathrm{i}=1,2)$ denote the power and phase of the different components, respectively. Introducing the phase difference $\phi_{\pm} = \phi_{1\pm} - \phi_{2\pm}$ we obtain the following set of equations:

$$\frac{dP_{1\pm}}{dz} = 2\kappa_{1\pm2+}\sqrt{P_{1\pm}P_{2\pm}}\sin\phi_{\pm}, \tag{4.5a}$$

$$\frac{dP_{2\pm}}{dz} = -2\kappa_{2\pm1+}\sqrt{P_{1\pm}P_{2\pm}}\sin\phi_{\pm}, \tag{4.5b}$$

$$\frac{d\phi_{1\pm}}{dz} = \frac{P_{1\pm}-P_{2\pm}}{\sqrt{P_{1\pm}P_{2\pm}}}\kappa_{1\pm2+}\cos\phi + \frac{4\kappa_{1\pm2+}}{P_{c\pm}}(P_{1\pm}-P_{2\pm}), \tag{4.6a}$$

$$\frac{d\phi_{2\pm}}{dz} = \frac{P_{1\pm}-P_{2\pm}}{\sqrt{P_{1\pm}P_{2\pm}}}\kappa_{2\pm1+}\cos\phi + \frac{4\kappa_{2\pm1+}}{P_{c\pm}}(P_{1\pm}-P_{2\pm}), \tag{4.6b}$$

here the critical power $P_{c\pm}$ is defined as $P_{c\pm} = 4\kappa_{1\pm2+}/\gamma(1-\delta)$. The set of Eqs. above can be solved analytically in terms of the elliptic function.

$$P_{1\pm}(z) = \frac{1}{2} P_0 [1 + \mathrm{cn}(2\kappa_{1\pm 2+}\, \mathrm{z} \,|\, m)\,, \tag{4.7a}$$

$$P_{2\pm}(z) = P_0 - P_{1\pm}(z)\,, \tag{4.7b}$$

where $z = L_c$ represents the coupling length of the chiral fiber coupler which can be given as $L_c = \pi / 2\kappa_{1\pm 2+}$ and $\mathrm{cn}(x \,|\, \mathrm{m})$ stand for Jacobi elliptic function with modulus $\mathrm{m}_{\pm} = (P_0 / P_{c\pm})^2$. where P_0 represent the initial input power for each component separately launched into fiber 1.

Under low input power condition, namely, $P_0 << P_{c\pm}$ $(\mathrm{m} << 1)$, the solution may be simplified to $P_{1\pm}(z) = P_0 \cos^2(\kappa_{1\pm 2+} z)$. When the power reaches the critical one with $P_0 = P_{c\pm}$ $(\mathrm{m} = 1)$, it reduces to $P_{1\pm}(z) = \frac{1}{2} P_0 \left(1 + \sec(2\kappa_{1\pm 2+} z)\right)$ and most power is transferred into the opposite fiber. If $P_0 > P_{ci\pm}$ $(\mathrm{m} > 1)$, the solution once again becomes periodic and most power is kept in the opposite fiber only with smaller fluctuations, which becomes negligible for $P_0 >> P_{ci\pm}$.

Figure 4.6 shows the switching curves, the relative output powers $P_{i\pm} / P_0$ $(i = 1,2)$ versus normalized input power $P_0 / P_{c\pm}$ in the different chirality strengths. In plotting the figure, the following parameters are used: the input power $(P_0 = 1\,\mathrm{W})$, wavelength $(\lambda = 1.55\,\mu\mathrm{m})$, core-radius of the fiber $(a = 2\lambda)$, nonlinear refractive index of the core $(n_2 = 3.5 \times 10^{-20}\,\mathrm{m}^2/\mathrm{W})$, the XPM parameter ($\delta = 2/3$), the effective cross-sectional area of the fiber $(A_{eff} = 60\,\mu\mathrm{m}^2)$ and the coupling length $(L_c = \pi / 2\kappa_{1\pm 2+})$.

Figure 4.6 (a) demonstrates the switching curves of $P_{i\pm} / P_0$ $(i = 1,2)$ versus $P_0 / P_{c\pm}$ for RCP and LCP components in both fibers with weak chirality strength $(\xi_c = 5 \times 10^{-6}\,\mathrm{mho})$. The complete switching occurs at $P_{0+} = 1.25 P_{c+}$ and $P_{0-} = 1.5 P_{c-}$ for RCP and LCP components, respectively, which can be calculated as P_{0+} =12.87 W and P_{0-} =16.97 W by definition of $P_{c\pm}$ through setting $\gamma = 20.0\ \mathrm{W^{-1}/km}$, $\kappa_{1+2+} = 0.17/\mathrm{cm}$ and $\kappa_{1-2+} = 0.18/\mathrm{cm}$. It is clear that the threshold of switching power for opposite components is different. From the Figure, one can see that the transition range from low state to high state is very short.

In the same ways, we calculated the threshold switching power for curves shown in Figure 4.6 (b) (P_{0c+}=4.13W and P_{0c-}=4.53 W), (c) (P_{0c+}=4.13W and P_{0c-}=4.53 W) and (d) (P_{0c+}=2.063W and P_{0c-}=2.72 W) for RCP and LCP components, respectively. These values indicate that as the chirality strength increases from $\xi_c = 1\times10^{-6}$ mho to $\xi_c = 8\times10^{-5}$ mho, the threshold switching power decrease P_{0c+}=12.87 W to P_{0c+}=2.063W and P_{0c-}=16.97 W to P_{0c-}=2.72 W for RCP and LCP components, correspondingly.

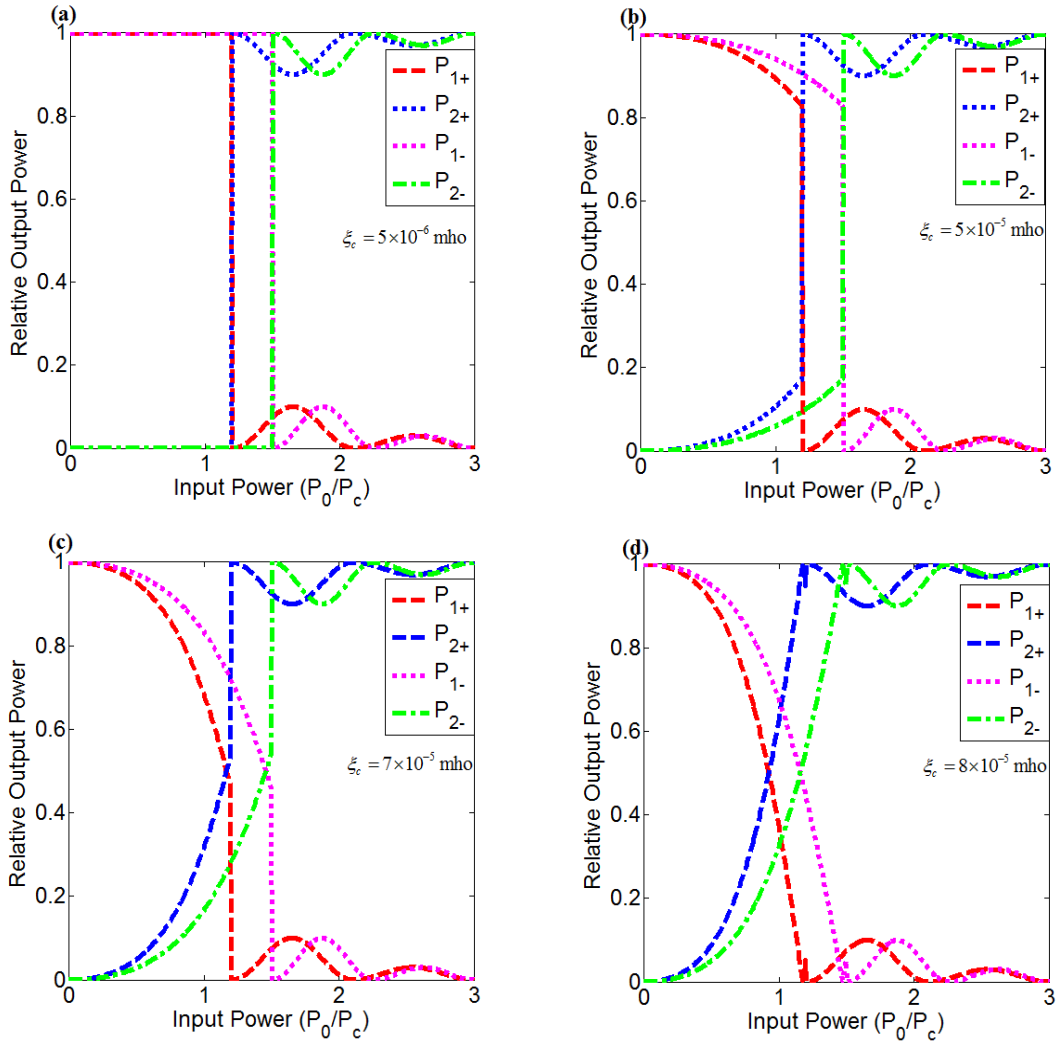

Figure 4.6 Nonlinear switching characteristics of chiral fiber couplers in waveguides 1 and 2 for RCP and LCP components

When the chirality strength ξ_c increases by one order of magnitude (say from 8×10^{-6} mho to 8×10^{-5}mho) as seen in Figure 4.6 (d) the low state becomes short while the high state shows more fluctuations and the transition range is wider than that in Figure 4.4 (a). It seems that the higher

states for RCP and LCP components are performed at the same points with that in Figure 4.4 (a), if we convert to real thresholds of switching power, however, they are reduced almost for one order of magnitude (P_{0+}=1.26 W and P_{0-}=1.66 W).

Based on these data, we noted the influence of the chirality strength effect in reducing the critical power threshold which is a good merit to make all-optical switching. On the other hand as the chirality strength increases, transition range increases, the switching time is longest, it is not suitable to make the fast optical switch. Thus, we recommended to use average chiral strength, say between $\xi_c = 1\times10^{-6}$ mho and $\xi_c = 8\times10^{-5}$ mho to make suitable fast optical all-optical switching.

4.3 Experimental Study on Nonlinear Chiral Optical Fiber Couplers

There has been quite much works on nonlinear effects in fiber and fiber couplers. In practical applications there are still many theoretical issues to be studied. To understand the detailed mechanisms of the nonlinear effects in fiber couplers, it is very crucial to investigate the effect experimentally. In this section, switching characteristics of nonlinear fiber couplers with different aspects in linear range were measured by using 100 fs high intensity laser beams at 1550 nm wavelength range. The nonlinear loss in fiber section was measured and analyzed and a characteristics power density for the nonlinear transform was estimated. Experimental results were coincident with the theoretical analysis and simulation obtained by using Runge-Kutta method.

The main elements of the experimental setup are indicated schematically in Figure 4.7. The source considered a titanium doped sapphire mode-looked laser and an optical parametric amplifier (OPA), provided pulses with 100 fs pulse-width and 1 kHz repetition rate. Its integrated spectrum was measured as shown in Figure 2, in which a fitted Gaussian curve was also shown as $U(\lambda) = U_0 \exp[-(\lambda - \lambda_p)^2 / (\Delta\lambda)^2]$ with peak wavelength of 1541 nm and 1/e maximum half line-width of 38 nm. The fitting was perfect except the low power pedestal parts, which meant that the laser pulse could be expected with good Gaussian waveform. From Fourier transformation limit relation, the pulse width could be estimated as $\tau \geq 0.4413/\Delta f \approx 56$ fs which was in a good agreement with the measured results by auto-correlation for Ti:sapphire 800 nm pulse of ~ 100 fs. The density cycle of the laser pulses was estimated to be about 10^{-10}.

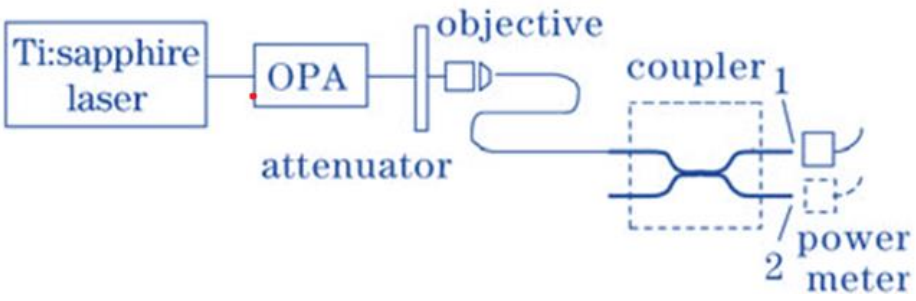

Figure 4.7 Experimental setup.

Figure 4.8 shows a curve in which the power of the left and right polarizing components of the two optical fiber under different parameters is transmitted with the length of the coupling. The initial condition we consider is that the left polarizing light of the radiation wavelength λ = 1.55μm is entered into the manual optical fiber 1. From Figure 4.8 (a), we can see that when the value of chiral parameter is small, the interaction between the left and right polarization components is so small through the joint interaction mechanism. In optical fiber 2, the cycle of the two polarization components is almost close, but there is a slight difference in the maximum amplitude value, while in optic fiber 1, the left and right polarizing components alternate cyclically.

As chirality value increases, this periodicity is broken, and the influence between the left and right circular polarization components increases. As can be seen in Figure 4.8 (b), the maximum power of the two circularly polarized components in Fiber 1 will also decrease with the increase of the coupling length, and the reduced power was coupled into the two components of Fiber 2. The maximum power of the two polarization components in fiber 2 has also increase, and they will suppress each other. Predominant, as shown in Figure 4.8 (c) predominant, as shown in Figure 4.8 (c). In this case, the power of the left-circularly polarized light in the two fibers will periodically overlap.

As can be seen from Figure 4.8 (d), when the chiral parameter is 0.001mho, only the left circular polarization component exists in the two fibers, and their transmission power alternates periodically, and when the coupling length is 0.026 mm, 0.052 mm, and 0.078 mm, the energy in fiber 1 will be completely coupled into fiber 2. When the coupling lengths are 0.013mm, 0.039mm, 0.065mm, respectively, the power in the two fibers is equal. Therefore, we can take advantage of this property of the chiral coupler to make a 3dB coupler for circularly polarized light by selecting the appropriate chiral parameters and coupling length.

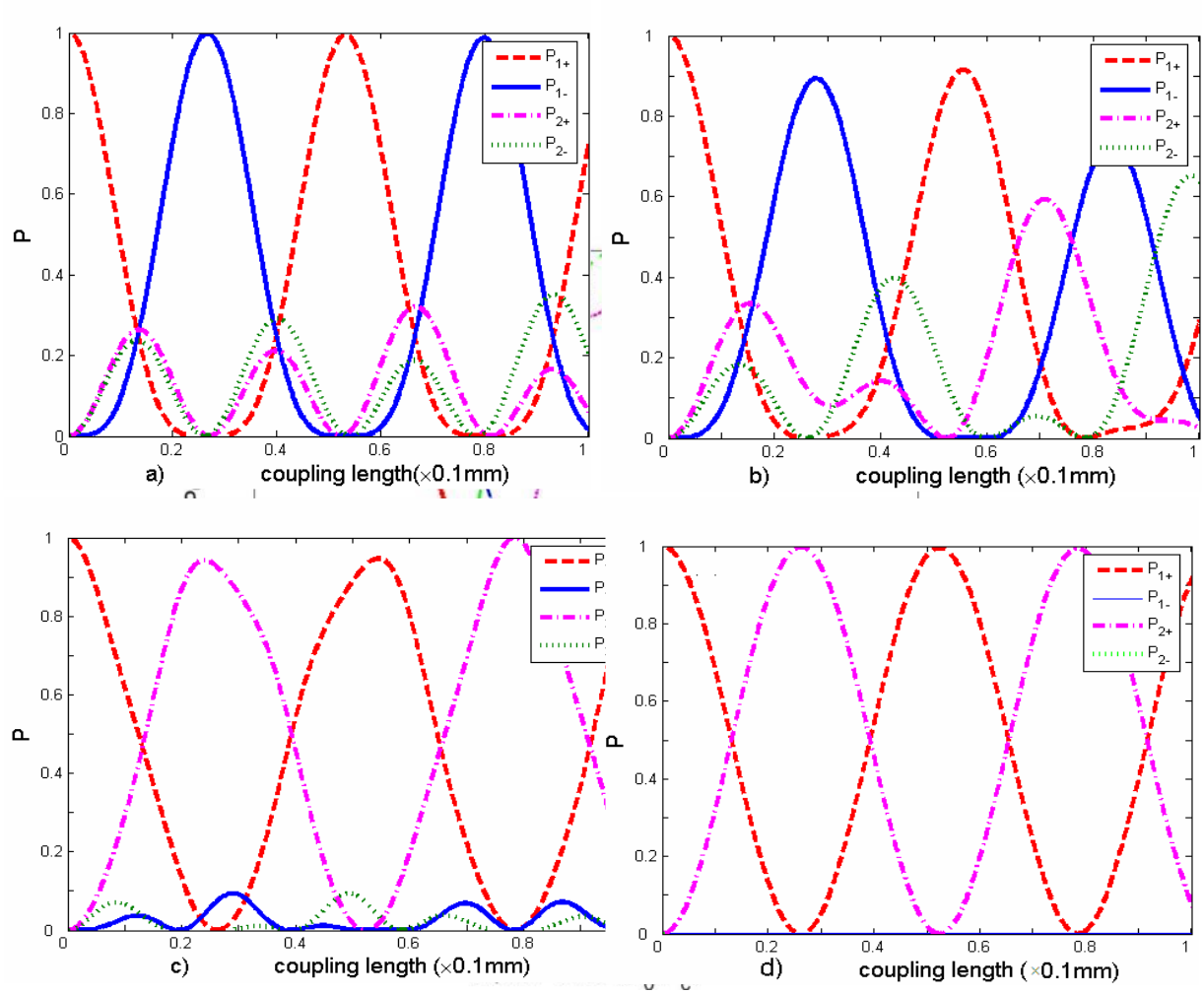

Figure 4.8 Experimental plot for the transmission power of LCP and RCP component in two arms of coupler versus coupling length for different chiral parameters: (a) ξc = 1×10^{-6}mho, (b) ξc = 1×10^{-5}mho, (c) ξc = 1×10^{-4} mho, (d) ξc = 1×10^{-3} mho.

Here, we need to show experimentally the characteristic of nonlinear fiber coupler by plotting curve. Figure 4.9 shows the switching curves, the relative output powers $P_{i\pm}/P_0$ $(i=1,2)$ versus normalized input power $P_0/P_{c\pm}$ with chirality strength. In plotting the figure, the following parameters are used: the input power $(P_0=1\,\mathrm{W})$, wavelength $(\lambda=1.55\,\mu\mathrm{m})$, core-radius of the fiber $(a=2\lambda)$, nonlinear refractive index of the core $(n_2=3.5\times10^{-20}\,\mathrm{m^2/W})$, the XPM parameter $(\delta=2/3)$, the effective cross-sectional area of the fiber $(A_{eff}=60\,\mu\mathrm{m}^2)$, $\xi_c = 8\times10^{-6}$ mho to 8×10^{-5}mho and the coupling length $(L_c=\pi/2\kappa_{1\pm2+})$. Figure 4.9 the low state becomes short while the high state shows more fluctuations and the transition range. It seems that the higher states for RCP and LCP components were performed.

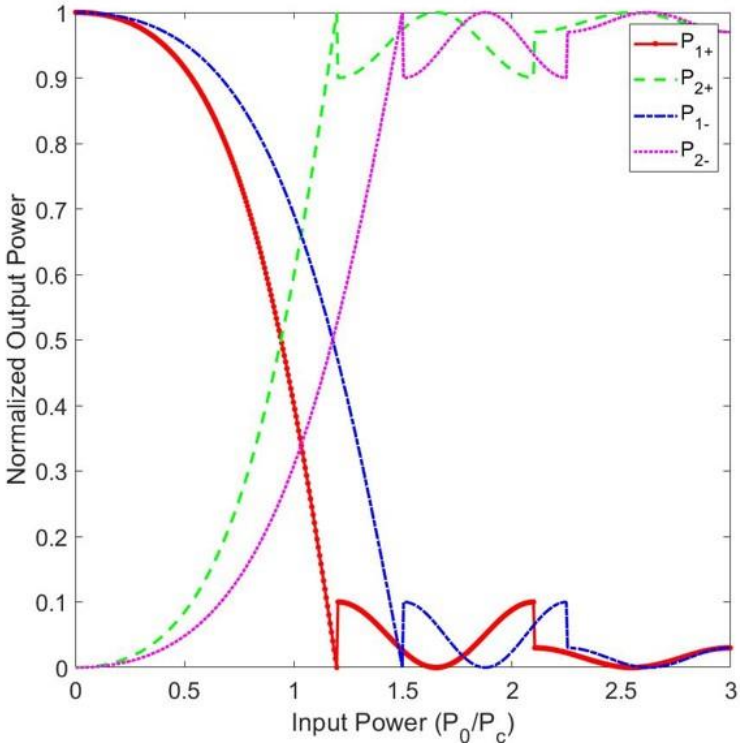

Figure 4.9 Experiment plot for nonlinear switching characteristics of chiral fiber couplers in waveguides 1 and 2 for RCP and LCP components

The experimental results were coincident with the simulations results as one can see from both Figure 4.6 (theoretical simulation) and Figure 4.9 (experimental). Nonlinear loss in fiber was also measured to get the injected power at the coupler. After deducting the nonlinear loss and input efficiency, the nonlinear switching critical peak powers for the couplers were calculated and the e result shows good agreement with its theoretical one.

5. Conclusion and Recommendation

Nonlinear fiber couplers made of chiral medium have different optical properties comparing to the achiral waveguides ones. The particular property is mainly reflected in the response of the polarization state of the light wave, which has a broad application prospect in optical fiber communication. In this paper, we have considered chiral nonlinear fiber couplers made of two identical cores and developed a comprehensive theory to describe the propagation of pulses through chiral nonlinear fiber couplers (NLFCs). Considering Maxwell's equations and Post's constitutive relations the Helmholtz's equations for chiral fiber is obtained. In the approximation of weak coupling, based on coupled-mode theory, the generalized coupled nonlinear Schrödinger equations (GCCNLSEs) of two chiral fibers are derived. The GCCNLSEs govern the evolution of left- and right-handed circularly polarized (LCP and RCP) components through dispersion and nonlinearity in cooperation with chirality. It is found that in GCCNLSEs chirality make a unique contribution to that of dispersion and nonlinearity.

The simulation is based on the Runge-Kutta method and numerical results reveal that the chirality can regulate the behavior of coupling and switching among the different components, which may provide an additional degree of freedom to distribute the optical information that is very vital in optical communication and remote sensing. The simulation has demonstrated that the chirality can regulate the behavior of coupling and switching among the different components, which may provide an additional degree of freedom to distribute the optical information that is very vital in optical communication and remote sensing. It is concluded that the chirality can provide an additional degree of freedom in optical device design that may find applications in optical communication and remote sensing.

We believed that current work might provide theoretical instruction for the researchers who are engaged in the chirality-related devices that can be used in optical communication and remote sensing.

6. References

[1] S. M. Jensen, "The nonlinear coherent coupler," *IEEE Transactions on Microwave Theory and Techniques,* vol. 30, pp. 1568-1571, 1982.

[2] C. Li, "All-Optical Switch Based on Nonlinear Optics," in *Nonlinear Optics*, ed: Springer, 2017, pp. 279-386.

[3] G. Agrawal, *Applications of nonlinear fiber optics*: Academic press, 2001.

[4] G. P. Agrawal, *Nonlinear fiber optics*: Academic press, 2007.

[5] J. Sitch, N. Mason, J. Roberts, and P. Robson, "All optical multiple-quantum-well waveguide switch," *Electronics Letters,* vol. 21, pp. 26-28, 1985.

[6] C. Li, *Nonlinear Optics: Principles and Applications*: Springer, 2016.

[7] L. A. Nafie, "Applications of Vibrational Optical Activity," *Vibrational Optical Activity: Principles and Applications,* pp. 293-333.

[8] J. J. Maki, M. Kauranen, and A. Persoons, "Surface second-harmonic generation from chiral materials," *Physical review B,* vol. 51, p. 1425, 1995.

[9] Y. Cao, J. Li, and Q. Su, "Guided modes in chiral fibers," *JOSA B,* vol. 28, pp. 319-324, 2011.

[10] L. D. Barron, *Molecular light scattering and optical activity*: Cambridge University Press, 2004.

[11] I. V. Lindell, A. Sihvola, S. Tretyakov, and A. Viitanen, "Electromagnetic waves in chiral and bi-isotropic media," 1994.

[12] P. Crabbe, "Optical Rotatory Dispersion and Circular Dicliroism in Organic Chemistry," 1965.

[13] R. A. Hegstrom and D. K. Kondepudi, "The handedness of the universe," *Scientific American,* vol. 262, pp. 108-115, 1990.

[14] P. Pelet and N. Engheta, "The theory of chirowaveguides," *IEEE Transactions on Antennas and Propagation,* vol. 38, pp. 90-98, 1990.

[15] !!! INVALID CITATION !!!

[16] X. Fang and R. O. Claus, "Polarization-independent all-fiber wavelength-division multiplexer based on a Sagnac interferometer," *Optics Letters,* vol. 20, pp. 2146-2148, 1995.

[17] P. H. Moose, "A technique for orthogonal frequency division multiplexing frequency offset correction," *IEEE Transactions on communications,* vol. 42, pp. 2908-2914, 1994.

[18] M.-F. Huang, J. Yu, and G.-K. Chang, "Polarization insensitive wavelength conversion for 4× 112Gbit/s polarization multiplexing RZ-QPSK signals," *Optics express,* vol. 16, pp. 21161-21169, 2008.

[19] P. Winzer, A. Gnauck, C. Doerr, M. Magarini, and L. Buhl, "Spectrally efficient long-haul optical networking using 112-Gb/s polarization-multiplexed 16-QAM," *Journal of lightwave technology,* vol. 28, pp. 547-556, 2010.

[20] C. A. Brackett, "Dense wavelength division multiplexing networks: Principles and applications," *IEEE Journal on Selected Areas in Communications,* vol. 8, pp. 948-964, 1990.

[21] Q. Zhao, H. Yin, and X. Chen, "Long-haul dense wavelength division multiplexing between a chaotic optical secure channel and a conventional fiber-optic channel," *Applied optics,* vol. 51, pp. 5585-5590, 2012.

[22] K. Saitoh and S. Matsuo, "Multicore fibers for large capacity transmission," *Nanophotonics,* vol. 2, pp. 441-454, 2013.

[23] E. B. Desurvire, "Capacity demand and technology challenges for lightwave systems in the next two decades," *Journal of Lightwave Technology,* vol. 24, pp. 4697-4710, 2006.

[24] S. Verdu, "A general formula for channel capacity," *IEEE Transactions on Information Theory,* vol. 40, pp. 1147-1157, 1994.

[25] R.-J. Essiambre, G. Kramer, P. J. Winzer, G. J. Foschini, and B. Goebel, "Capacity limits of optical fiber networks," *Journal of Lightwave Technology,* vol. 28, pp. 662-701, 2010.

[26] W. L. Barnes, W. A. Murray, J. Dintinger, E. Devaux, and T. Ebbesen, "Surface plasmon polaritons and their role in the enhanced transmission of light through periodic arrays of subwavelength holes in a metal film," *Physical review letters,* vol. 92, p. 107401, 2004.

[27] W. L. Barnes, A. Dereux, and T. W. Ebbesen, "Surface plasmon subwavelength optics," *nature,* vol. 424, p. 824, 2003.

[28] E. J. Smith, Z. Liu, Y. Mei, and O. G. Schmidt, "Combined surface plasmon and classical waveguiding through metamaterial fiber design," *Nano letters,* vol. 10, pp. 1-5, 2009.

[29] H.-T. Chen, W. J. Padilla, J. M. Zide, A. C. Gossard, A. J. Taylor, and R. D. Averitt, "Active terahertz metamaterial devices," *Nature,* vol. 444, p. 597, 2006.

[30] N. M. Litchinitser, "Structured light meets structured matter," *Science,* vol. 337, pp. 1054-1055, 2012.

[31] K. Bi, Y. Guo, J. Zhou, G. Dong, H. Zhao, Q. Zhao, *et al.*, "Negative and near zero refraction metamaterials based on permanent magnetic ferrites," *Scientific reports,* vol. 4, p. 4139, 2014.

[32] H. Chen, W. J. Padilla, R. D. Averitt, J. F. O'hara, and M. Lee, "Active terahertz metamaterial devices," ed: Google Patents, 2010.

[33] K. Bi, Y. Guo, J. Zhou, G. Dong, H. Zhao, Q. Zhao, *et al.*, "Negative and near zero refraction metamaterials based on permanent magnetic ferrites," *Sci. Rep,* vol. 4, p. 4139, 2014.

[34] D. Gelmecha, J.-Q. Li, and M. Teklu, "Pulse propagation with self-phase modulation in nonlinear chiral fiber and its applications," *Chinese Physics Letters,* vol. 33, p. 094202, 2016.

[35] J. Pendry, "A chiral route to negative refraction," *Science,* vol. 306, pp. 1353-1355, 2004.

[36] J. B. Pendry, "Negative refraction makes a perfect lens," *Physical review letters,* vol. 85, p. 3966, 2000.

[37] I. V. Shadrivov, A. A. Sukhorukov, and Y. S. Kivshar, "Complete band gaps in one-dimensional left-handed periodic structures," *Physical review letters,* vol. 95, p. 193903, 2005.

[38] S. Atakaramians, A. Argyros, S. C. Fleming, and B. T. Kuhlmey, "Hollow-core waveguides with uniaxial metamaterial cladding: modal equations and guidance conditions," *JOSA B,* vol. 29, pp. 2462-2477, 2012.

[39] R. Ruppin, "Surface polaritons of a left-handed medium," *Physics Letters A,* vol. 277, pp. 61-64, 2000.

[40] Z. H. Wang, Z. Y. Xiao, and W. Y. Luo, "Surface modes in left-handed material slab waveguides," *Journal of Optics A: Pure and Applied Optics,* vol. 11, p. 015101, 2008.

[41] J. Lægsgaard, O. Bang, and A. Bjarklev, "Photonic crystal fiber design for broadband directional coupling," *Optics letters,* vol. 29, pp. 2473-2475, 2004.

[42] R. Cregan, B. Mangan, J. Knight, T. Birks, P. S. J. Russell, P. Roberts, *et al.*, "Single-mode photonic band gap guidance of light in air," *Science,* vol. 285, pp. 1537-1539, 1999.

[43] D. Lin, P. Fan, E. Hasman, and M. L. Brongersma, "Dielectric gradient metasurface optical elements," *Science,* vol. 345, pp. 298-302, 2014.

[44] H.-T. Chen, W. J. Padilla, J. M. Zide, A. C. Gossard, A. J. Taylor, and R. D. Averitt, "Active terahertz metamaterial devices," *Nature,* vol. 444, pp. 597-600, 2006.

[45] N. Bozinovic, Y. Yue, Y. Ren, M. Tur, P. Kristensen, H. Huang, *et al.*, "Terabit-scale orbital angular momentum mode division multiplexing in fibers," *Science,* vol. 340, pp. 1545-1548, 2013.

[46] J. Wang, J.-Y. Yang, I. M. Fazal, N. Ahmed, Y. Yan, H. Huang, *et al.*, "Terabit free-space data transmission employing orbital angular momentum multiplexing," *Nature Photonics,* vol. 6, pp. 488-496, 2012.

[47] G. Wong, M. Kang, H. Lee, F. Biancalana, C. Conti, T. Weiss, *et al.*, "Excitation of orbital angular momentum resonances in helically twisted photonic crystal fiber," *Science,* vol. 337, pp. 446-449, 2012.

[48] G. H. Wagnière, *On chirality and the universal asymmetry: reflections on image and mirror image*: John Wiley & Sons, 2008.

[49] J. Broeng, D. Mogilevstev, S. E. Barkou, and A. Bjarklev, "Photonic crystal fibers: A new class of optical waveguides," *Optical fiber technology,* vol. 5, pp. 305-330, 1999.

[50] L. Poladian, M. Straton, A. Docherty, and A. Argyros, "Pure chiral optical fibres," *Optics express,* vol. 19, pp. 968-980, 2011.

[51] E. Plum, "Chirality and metamaterials," University of Southampton, 2010.

[52] E. Plum, V. Fedotov, and N. Zheludev, "Extrinsic electromagnetic chirality in metamaterials," *Journal of Optics A: Pure and Applied Optics,* vol. 11, p. 074009, 2009.

[53] E. Plum, V. Fedotov, and N. Zheludev, "Optical activity in extrinsically chiral metamaterial," *Applied physics letters,* vol. 93, p. 191911, 2008.

[54] E. Plum, X.-X. Liu, V. Fedotov, Y. Chen, D. Tsai, and N. Zheludev, "Metamaterials: optical activity without chirality," *Physical review letters,* vol. 102, p. 113902, 2009.

[55] A. s. E. Leal, A. n. Rubio, and S. Infm-cnr, "Ab initio Study of the Optical Activity in Chiral Systems," Citeseer, 2009.

[56] Y. Liu and X. Zhang, "Metamaterials: a new frontier of science and technology," *Chemical Society Reviews,* vol. 40, pp. 2494-2507, 2011.

[57] D. R. Smith, J. B. Pendry, and M. C. Wiltshire, "Metamaterials and negative refractive index," *Science,* vol. 305, pp. 788-792, 2004.

[58] J. B. Pendry, A. Holden, W. Stewart, and I. Youngs, "Extremely low frequency plasmons in metallic mesostructures," *Physical review letters,* vol. 76, p. 4773, 1996.

[59] J. B. Pendry, A. J. Holden, D. J. Robbins, and W. Stewart, "Magnetism from conductors and enhanced nonlinear phenomena," *IEEE transactions on microwave theory and techniques,* vol. 47, pp. 2075-2084, 1999.

[60] D. R. Smith and N. Kroll, "Negative refractive index in left-handed materials," *Physical Review Letters,* vol. 85, p. 2933, 2000.

[61] H. Chen, Z. Wang, R. Zhang, H. Wang, S. Lin, F. Yu, *et al.*, "A meta-substrate to enhance the bandwidth of metamaterials," *Scientific reports,* vol. 4, p. 5264, 2014.

[62] J. Valentine, S. Zhang, T. Zentgraf, E. Ulin-Avila, D. A. Genov, G. Bartal, *et al.*, "Three-dimensional optical metamaterial with a negative refractive index," *nature,* vol. 455, p. 376, 2008.

[63] J. Zhou, J. Dong, B. Wang, T. Koschny, M. Kafesaki, and C. M. Soukoulis, "Negative refractive index due to chirality," *Physical Review B,* vol. 79, p. 121104, 2009.

[64] S. Zhang, Y.-S. Park, J. Li, X. Lu, W. Zhang, and X. Zhang, "Negative refractive index in chiral metamaterials," *Physical review letters,* vol. 102, p. 023901, 2009.

[65] J. K. Gansel, M. Thiel, M. S. Rill, M. Decker, K. Bade, V. Saile, *et al.*, "Gold helix photonic metamaterial as broadband circular polarizer," *Science,* vol. 325, pp. 1513-1515, 2009.

[66] C. Menzel, C. Helgert, C. Rockstuhl, E.-B. Kley, A. Tünnermann, T. Pertsch, *et al.*, "Asymmetric transmission of linearly polarized light at optical metamaterials," *Physical review letters,* vol. 104, p. 253902, 2010.

[67] V. Fedotov, P. Mladyonov, S. Prosvirnin, A. Rogacheva, Y. Chen, and N. Zheludev, "Asymmetric propagation of electromagnetic waves through a planar chiral structure," *Physical review letters,* vol. 97, p. 167401, 2006.

[68] D. Wen, F. Yue, G. Li, G. Zheng, K. Chan, S. Chen, *et al.*, "Helicity multiplexed broadband metasurface holograms," *Nature communications,* vol. 6, 2015.

[69] D. Wen, F. Yue, G. Li, G. Zheng, K. Chan, S. Chen, *et al.*, "Helicity multiplexed broadband metasurface holograms," *Nature communications,* vol. 6, p. 8241, 2015.

[70] A. Lakhtakia, V. V. Varadan, and V. K. Varadan, "Field equations, Huygens's principle, integral equations, and theorems for radiation and scattering of electromagnetic waves in isotropic chiral media," *JOSA A*, vol. 5, pp. 175-184, 1988.

[71] G. Y. Slepyan, S. Maksimenko, A. Lakhtakia, O. Yevtushenko, and A. Gusakov, "Electrodynamics of carbon nanotubes: Dynamic conductivity, impedance boundary conditions, and surface wave propagation," *Physical Review B*, vol. 60, p. 17136, 1999.

[72] D. Jaggard, A. Mickelson, and C. Papas, "On electromagnetic waves in chiral media," *Applied physics*, vol. 18, pp. 211-216, 1979.

[73] H. Ammari and J. Nédélec, *Time-harmonic electromagnetic fields in chiral media*: Citeseer, 1996.

[74] S. Bassiri, C. Papas, and N. Engheta, "Electromagnetic wave propagation through a dielectric–chiral interface and through a chiral slab," *JOSA A*, vol. 5, pp. 1450-1459, 1988.

[75] N. Engheta and P. Pelet, "Modes in chirowaveguides," *Optics Letters*, vol. 14, pp. 593-595, 1989.

[76] J. A. Svedin, "Propagation analysis of chirowaveguides using the finite-element method," *IEEE transactions on Microwave Theory and Techniques*, vol. 38, pp. 1488-1496, 1990.

[77] P. Pelet and N. Engheta, "Coupled-mode theory for chirowaveguides," *Journal of Applied Physics*, vol. 67, pp. 2742-2745, 1990.

[78] S. F. Mahmoud, "Guided modes on open chirowaveguides," *IEEE transactions on microwave theory and techniques*, vol. 43, pp. 205-209, 1995.

[79] R. C. Qiu and I.-T. Lu, "Guided waves in chiral optical fibers," *JOSA A*, vol. 11, pp. 3212-3219, 1994.

[80] A. Singh, K. S. Singh, P. Khastgir, S. Ojha, and O. Singh, "Modal cutoff condition of an optical chiral fiber with different chiralities in the core and the cladding," *JOSA B*, vol. 11, pp. 1283-1287, 1994.

[81] F. M. Janeiro, C. R. Paiva, and A. L. Topa, "Guidance and leakage properties of chiral optical fibers," *JOSA B*, vol. 19, pp. 2558-2566, 2002.

[82] L. Jun-Qing, L. She, W. Xiao-Ou, Z. Yang-Dong, and L. Chun-Fei, "Self-induced optical rotation of solitons in a chiral fibre," *Chinese Physics Letters*, vol. 21, p. 675, 2004.

[83] A. Argyros, M. Straton, A. Docherty, E. H. Min, Z. Ge, K. H. Wong, *et al.*, "Consideration of chiral optical fibres," *Frontiers of Optoelectronics in China,* vol. 3, pp. 67-70, 2010.

[84] J. Dong, "Guided and surface modes in chiral nihility fiber," *Optics Communications,* vol. 283, pp. 532-536, 2010.

[85] Y. Cao, J. Li, and Q. Su, "Guided modes in chiral fibers: erratum," *JOSA B,* vol. 30, pp. 1232-1233, 2013.

[86] Y. Cao and J. Li, "Modal bifurcation in chiral multilayered fibers," *JOSA B,* vol. 30, pp. 2168-2173, 2013.

[87] Y. Cao and J. Li, "Transverse electromagnetic modes in chiral negatively refractive fibers and a new type of space-division multiplexing," *Optics letters,* vol. 39, pp. 255-258, 2014.

[88] P. Fischer and F. Hache, "Nonlinear optical spectroscopy of chiral molecules," *Chirality,* vol. 17, pp. 421-437, 2005.

[89] H. Mesnil and F. Hache, "Experimental evidence of third-order nonlinear dichroism in a liquid of chiral molecules," *Physical review letters,* vol. 85, p. 4257, 2000.

[90] R. W. Boyd, J. E. Sipe, and P. W. Milonni, "Chirality and polarization effects in nonlinear optics," *Journal of Optics A: Pure and Applied Optics,* vol. 6, p. S14, 2004.

[91] A. Persoons, M. Kauranen, S. V. Elshocht, T. Verbiest, L. Ma, L. Pu, *et al.*, "Chiral effects in second-order nonlinear optics," *Molecular Crystals and Liquid Crystals Science and Technology. Section A. Molecular Crystals and Liquid Crystals,* vol. 315, pp. 93-98, 1998.

[92] Z. Bi, D. Chao-Qing, and Z. Jie-Fang, "Self-Similar Vortex Solitons for the Distributed-Coefficient Nonlinear Schrödinger Equation," *Chinese Physics Letters,* vol. 29, p. 084201, 2012.

[93] J. Li, Q. Su, and Y. Cao, "Circularly polarized guided modes in dielectrically chiral photonic crystal fiber," *Optics letters,* vol. 35, pp. 2720-2722, 2010.

[94] Z. C. Tiu, S. J. Tan, A. Zarei, H. Ahmad, and S. W. Harun, "Nonlinear polarization rotation-based mode-locked Erbium-doped fiber laser with three switchable operation states," *Chinese Physics Letters,* vol. 31, p. 094206, 2014.

[95] C. Jun-Chao, Z. Xiao-Fei, L. Biao, and C. Yong, "Exact solutions to the two-dimensional spatially inhomogeneous cubic-quintic nonlinear Schrödinger equation with an external potential," *Chinese Physics Letters*, vol. 29, p. 070303, 2012.

[96] H. Torres-Silva and M. Zamorano, "Chiral effects on optical solitons," *Mathematics and computers in simulation*, vol. 62, pp. 149-161, 2003.

[97] N. J. Zabusky and M. D. Kruskal, "Interaction of" solitons" in a collisionless plasma and the recurrence of initial states," *Physical review letters*, vol. 15, p. 240, 1965.

[98] Z. Mezache and F. Benabdelaziz, "Study of chiroptical fiber nonlinearities with new formulation of constitutive equations," *Journal of Electromagnetic Waves and Applications*, vol. 29, pp. 2257-2268, 2015.

[99] Z. Mezache, S. Aib, F. Benabdelaziz, and C. Zebiri, "Modeling of a light pulse in bi-isotropic optical fiber with Kerr effect: case of Tellegen media," *Nonlinear Dynamics*, vol. 86, pp. 789-794, 2016.

[100] V. I. Kopp, "Chiral fibers," in *Optical Fiber Communication Conference*, 2013, p. OTu2G. 5.

[101] E. Plum, J. Zhou, J. Dong, V. Fedotov, T. Koschny, C. Soukoulis, *et al.*, "Metamaterial with negative index due to chirality," *Physical Review B*, vol. 79, p. 035407, 2009.

[102] D. Jaggard, A. Mickelson, and C. Papas, "On electromagnetic waves in chiral media," *Applied Physics A: Materials Science & Processing*, vol. 18, pp. 211-216, 1979.

[103] A. W. Snyder, "Coupled-mode theory for optical fibers," *JOSA*, vol. 62, pp. 1267-1277, 1972.

[104] A. Yariv, "Coupled-mode theory for guided-wave optics," *IEEE Journal of Quantum Electronics*, vol. 9, pp. 919-933, 1973.

[105] R. Nayak, "Analysis of Optical Soliton Propagation in Birefringent Fibers," *International Journal of Managment, IT and Engineering*, vol. 2, pp. 96-102, 2012.

[106] N. Trivunac-Vukovic and B. Milovanovic, "FDTD simulation of all-optical switch using different wavelength controlling pulse in the NLDC," in *Electrotechnical Conference, 2000. MELECON 2000. 10th Mediterranean*, 2000, pp. 269-272.

[107] E. Alkan, V. Demir, A. Z. Elsherbeni, and E. Arvas, "Dual-grid finite-difference frequency-domain method for modeling chiral medium," *IEEE Transactions on Antennas and Propagation*, vol. 58, pp. 817-823, 2010.

[108] R. A. Fisher and W. K. Bischel, "Numerical studies of the interplay between self-phase modulation and dispersion for intense plane-wave laser pulses," *Journal of Applied Physics,* vol. 46, pp. 4921-4934, 1975.

[109] M. Barnoski, *Fundamentals of optical fiber communications*: Elsevier, 2012.

[110] P. P. Banerjee, *Nonlinear optics: theory, numerical modeling, and applications*: CRC Press, 2003.

[111] K. Okamoto, *Fundamentals of optical waveguides*: Academic press, 2010.

[112] J. S. Walker, "Fourier analysis and wavelet analysis," *Notices of the AMS,* vol. 44, pp. 658-670, 1997.

[113] J. L. Volakis, A. Chatterjee, and L. C. Kempel, *Finite element method electromagnetics: antennas, microwave circuits, and scattering applications* vol. 6: John Wiley & Sons, 1998.

[114] J. Jin, "The Finite Element Method in Electromagnetics, John Willey & Sons," *Inc., New York,* 2002.

[115] S. V. BALASUBRAMANIAM, "FINITE ELEMENT ANALYSIS OF LEFT-HANDED WAVEGUIDES," University of Central Florida Orlando, Florida, 2004.

[116] F. Bréchet, J. Marcou, D. a. Pagnoux, and P. Roy, "Complete analysis of the characteristics of propagation into photonic crystal fibers, by the finite element method," *Optical Fiber Technology,* vol. 6, pp. 181-191, 2000.

[117] M. Qiu, "Analysis of guided modes in photonic crystal fibers using the finite-difference time-domain method," *Microwave and Optical Technology Letters,* vol. 30, pp. 327-330, 2001.

[118] C. J. Ryu, A. Y. Liu, E. Wei, and W. C. Chew, "Finite-Difference Time-Domain Simulation of the Maxwell–Schrödinger System," *IEEE Journal on Multiscale and Multiphysics Computational Techniques,* vol. 1, pp. 40-47, 2016.